INTERNATIONAL JOURNAL FOR NUMERICAL METHODS IN FLUIDS
Int. J. Numer. Meth. Fluids 2004; **45**:197–229 (DOI: 10.1002/fld.685)

Implicit WENO shock capturing scheme for unsteady flows. Application to one-dimensional Euler equations

A. Cadiou[1,*,†] and C. Tenaud[2]

[1]*LMFA, UMR CNRS 5509, 36 Av. Guy de Collongue, 69131 Ecully, France*
[2]*LIMSI, UPR CNRS 3251 B.P. 133, 91403 Orsay Cedex, France*

SUMMARY

The unsteady numerical simulation of one-dimensional shock waves is investigated using high-order convective TVD and WENO schemes. Emphasis is put on the capability of existing explicit and implicit time discretization to capture the correct shock velocity. A new implicit solver is then proposed based on the WENO approach. This scheme is presented for one-dimensional problems, but is easily extended to multi-dimensional cases. The implicit WENO scheme is tested against the classical TVD schemes for the case of the shock tube and shock-entropy wave interaction. Copyright © 2004 John Wiley & Sons, Ltd.

KEY WORDS: implicit solver; shock capturing scheme; TVD condition; WENO approach

1. INTRODUCTION

High-order resolution of non-linear hyperbolic systems of conservation laws is of interest in practical applications of compressible aerodynamic turbulent flows involving both shock and smooth structures. The resolution of the corresponding convection–diffusion equations is generally based on an operator splitting formulation where the hyperbolic part and the parabolic part are treated separately. This formulation is particularly useful when one desires to apply high-order spatial resolution of the convective term and an efficient implicit discretization of the diffusive terms. However, the splitting method generates a temporal splitting error [1], thereby imposing a time-step restriction that can be more severe than the one needed to resolve the viscous waves. It is, therefore, interesting to develop implicit solvers for high-order resolution of the convective part that can be calculated with the same time step as the viscous

*Correspondence to: A. Cadiou, LMFA, UMR CNRS 5509, 36 Av. Guy de Collongue, 69131 Ecully, France.
†E-mail: Anne.Cadiou@ec-lyon.fr

Received 27 December 2002
Revised 21 October 2003

term. This study is focussed on the development and evaluation of an implicit solver based on a high-order spatial convective scheme for the resolution of an unsteady hyperbolic system.

To avoid the generation of oscillations across discontinuities of the solution, total variation diminishing (TVD) schemes have been extensively developed for fluid dynamic problems [2–5]. These schemes are second-order accurate for bounded smooth problems [6]. The TVD property is obtained by means of slope [7] or flux limiters [8, 9] which enforce monotonicity of the solution. Unfortunately, these limiters render the TVD schemes highly non-linear. The extension of explicit to implicit TVD schemes involves linearization of the spatial operator that has to satisfy conservative properties of the continuous hyperbolic system in order to deal with unsteady flows [10]. As a result, the implicit scheme may no longer be unconditionally TVD. Despite these difficulties, explicit and implicit TVD schemes have been widely applied to solve Euler and Navier–Stokes equations.

An other class of high-order shock capturing schemes is based on the essentially non-oscillatory (ENO) approach developed by Harten *et al.* [11] and Shu and Osher [12, 13]. These schemes are based on the selection of the smoothest stencil among several candidates to approximate fluxes at cell boundaries to get a high order and oscillation-free solution near discontinuities. ENO schemes can be of order higher than two. In order to get over a free adaptation of the stencil, weighted ENO (WENO) schemes have been developed by Liu *et al.* [14] and Jiang and Shu [15] that are based on a convex combination of all candidate stencils. Explicit WENO schemes have been extensively applied to compressible Euler and Navier–Stokes equations, in combination with a class of high-order Runge–Kutta methods that maintain stability properties of the spatial operator [12]. Recently, an implicit resolution of the WENO scheme of Jiang and Shu has been proposed by Chen *et al.* [16] and applied to the resolution of incompressible steady-state and time-dependent flows. Yang *et al.* [17] have extended this method to the resolution of steady compressible Navier–Stokes equations. In both approaches, the construction of the implicit operator follows the approach usually retained for TVD schemes. Implicit TVD schemes are second-order accurate and degenerate to first order at smooth extrema. When such an implicit operator is applied to WENO schemes, the resulting schemes remain second-order accurate everywhere, no matter what the accuracy of the corresponding explicit WENO schemes might be. In the present study, a method specific to the WENO approach is developed. The purpose of this paper is to show that the implicit operator remains stable and accurate, while no numerically dissipative term is introduced in the operator. The approximation that were suitable for steady-state flows are shown to be too restrictive for unsteady flows involving shocks and contact discontinuities. The method proposed here focusses on the ability of capturing the correct shock velocity. It is presented in a one-dimensional approximation, but it will be shown to be easily extended to multiple space dimensions.

The governing equations and the notations used in this paper are presented in Section 2. Section 3 details the time and space discretizations investigated in this study. First, the explicit form of TVD and WENO schemes are described for the sake of completeness. The proposed construction of the implicit operator used with the WENO scheme is then presented and the resulting operator is compared with the more classical one usually associated with the TVD scheme. Section 4 presents the results obtained with these schemes in two one-dimensional cases, the shock tube and the shock-entropy wave interaction. Final conclusions are given in Section 5.

2. GOVERNING EQUATIONS

The unsteady compressible Euler equations of gas dynamics can be written as

$$\frac{\partial \mathbf{Q}}{\partial t} + \nabla.\mathbf{F} = 0 \tag{1}$$

where $\mathbf{Q}$ is the conservative variable vector and $\mathbf{F}$ the convective flux defined in one-dimensional cases as

$$\mathbf{Q} = \begin{bmatrix} \rho \\ \rho u \\ \rho e \end{bmatrix} \quad \text{and} \quad \mathbf{F} = \begin{bmatrix} \rho u \\ \rho u^2 + p \\ u(\rho e + p) \end{bmatrix}$$

where ρ is the density, u the velocity and e the specific total energy. Assuming a perfect gas, the latter can be expressed in terms of the static pressure p by

$$e = \frac{p}{\rho(\gamma - 1)} + \frac{1}{2} u^2$$

and $\gamma = 1.4$ is the ratio of specific heat coefficient for air. The system of equations is closed using the perfect gas relationship $p = \rho RT$ where R is a constant obtained by dividing the universal gas constant by the molecular weight of the gas.

3. NUMERICAL APPROACH

3.1. Curvilinear co-ordinates

The governing equations are discretized by a finite volume approach. The one-dimensional domain applied here is rather simple but may involve curvature and non-uniformities in the physical space. A generalized co-ordinate transformation is therefore applied to take into account non-uniform but smooth meshes. This transformation is presented in multi-dimensional space to preserve the generality of the method.

In order to take into account a non-uniform distribution of mesh points in the physical space, see Figure 1, spatial operators are calculated in a transformed plane, or computational domain, see Figure 2, where the mesh step size is unity. The co-ordinate transformation from the cartesian co-ordinates x^j to the curvilinear co-ordinates ξ^i is defined by the metric tensor

$$b_j^i = J \frac{\partial \xi^i}{\partial x^j}$$

where J is the Jacobian of the transformation. The vectors $\mathbf{b}^i$ are surface-oriented normals of the iso-lines ξ^i. This co-ordinate transformation leads to the following expression of the divergence operator:

$$\nabla.\mathbf{F} = \frac{1}{J} \frac{\partial}{\partial \xi^i} [b_j^i \; F^j] \tag{2}$$

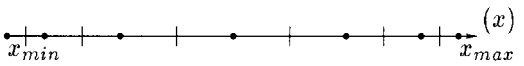

Figure 1. Physical domain.

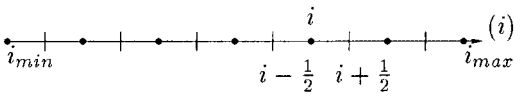

Figure 2. Computational domain.

where F^j is the jth cartesian component of the convective flux. Hence, the flux is decomposed in each direction of the computational domain in the following contravariant components:

$$f^i = b^i_j F^j$$

so that the Euler equations write

$$\frac{\partial \mathbf{Q}}{\partial t} = -\frac{1}{J}\frac{\partial}{\partial \xi^i}[\mathbf{f}^i] \tag{3}$$

In one-dimensional calculations, the transformation links only x to ξ. The normal vector of the cell interface does not depend on the cell localization and can therefore be considered as equal to unity and oriented along the x-axis. The only non-zero component of $\mathbf{b}^1$ is b^1_1, which is written as

$$b^1_1 = J\frac{\partial \xi}{\partial x} \tag{4}$$

where J, the Jacobian of the transformation, characterizes the volume variation of the cells. It is defined here as

$$J = \frac{\partial x}{\partial \xi} \tag{5}$$

and setting $\mathbf{f} \equiv f^1$, the Euler equations become

$$\frac{\partial \mathbf{Q}}{\partial t} = -\frac{1}{J}\frac{\partial}{\partial \xi}[\mathbf{f}] \tag{6}$$

The numerical resolution of, respectively, the time-dependent and spatial operators in Equation (6) is discussed in the following sections.

3.2. Time discretization

The governing equations can be written as a system of ordinary differential equations (ODE):

$$\frac{\partial \mathbf{Q}}{\partial t} = -\frac{1}{J}L(\mathbf{Q}) \tag{7}$$

where $L(\mathbf{Q})$ is the discretized spatial operator. Two approaches to advance the solution at time t^n noted by $\mathbf{Q}^n$ to the next timestep at t^{n+1} are investigated here. One consists in the

explicit resolution of the equations where $\mathbf{Q}^{n+1}$ is written in terms of the previous time states and the other by an implicit scheme. Explicit and implicit calculations are performed at fixed CFL number in order to compare the different approaches. The physical time step is expressed in terms of the most restrictive CFL number, imposed by the stability criteria of the explicit scheme.

3.2.1. Explicit scheme. The explicit time scheme used here is the third order TVD Runge–Kutta method developed by Shu and Osher [12]. This scheme, expressed in terms of increments over $\mathbf{Q}^n$ states, writes:

$$\Delta\mathbf{Q}^{(1)} = \Delta t^{n+1}\left[-\frac{1}{J}L(\mathbf{Q}^n)\right] \tag{8a}$$

$$\Delta\mathbf{Q}^{(2)} = \frac{1}{4}\Delta\mathbf{Q}^{(1)} + \frac{1}{4}\Delta t^{n+1}\left[-\frac{1}{J}L(\mathbf{Q}^{(1)})\right] \tag{8b}$$

$$\Delta\mathbf{Q}^{n+1} = \frac{2}{3}\Delta\mathbf{Q}^{(2)} + \frac{2}{3}\Delta t^{n+1}\left[-\frac{1}{J}L(\mathbf{Q}^{(2)})\right] \tag{8c}$$

where $\Delta t^{n+1} = t^{n+1} - t^n$ denotes the time step and $\Delta\mathbf{Q}^{n+1} = \mathbf{Q}^{n+1} - \mathbf{Q}^n$ is the increment in the solution vector. This scheme is TVD and therefore consistent with shock capturing schemes [18]. It will be further referred to as RK. This scheme is stable under a CFL restriction: for TVD [4] and $r = 3$ WENO schemes [15] the limit CFL $= 1$ is usual.

Time scheme	Ref.	Order $O(\Delta t^n)$	CFL max
TVD Runge–Kutta	RK	3	1

3.2.2. Implicit scheme. A general semi-implicit linear multi-step scheme can be written as [19, 20]:

$$(1+\beta)\frac{\Delta\mathbf{Q}^{n+1}}{\Delta t^{n+1}} = \beta\frac{\Delta\mathbf{Q}^{n}}{\Delta t^{n}} - \frac{1}{J}[\theta L(\mathbf{Q}^{n+1}) + (1-\theta+\phi)L(\mathbf{Q}^n) - \phi L(\mathbf{Q}^{n-1})] \tag{9}$$

This scheme is second-order accurate if the following relation is satisfied:

$$\beta = (2\theta - 1)\frac{\Delta t^{n+1}}{\Delta t^{n+1} + \Delta t^n} + 2\phi\frac{\Delta t^n}{\Delta t^{n+1} + \Delta t^n} \tag{10a}$$

When $\phi = 0$, the only free parameter is θ which defines the relative importance of implicit over explicit terms. A third-order scheme is obtained when Equation (10a) is satisfied together with:

$$\theta = \frac{\Delta t^n}{\Delta t^{n+1} + 2\Delta t^n} + \phi\frac{\Delta t^n}{\Delta t^{n+1}}\frac{\Delta t^n + 2\Delta t^{n+1}}{\Delta t^{n+1} + 2\Delta t^n} \tag{10b}$$

Table I. Overview of implicit time schemes.

Time scheme	Ref.	θ	β	ϕ	Order $O(\Delta t^n)$	CFL max
Explicit Euler	EE	0	0	0	1	1
Trapeze	T	0.5	0	0	2	2
Upwind Euler	ER	1	$\dfrac{\Delta t^{n+1}}{\Delta t^{n+1}+\Delta t^n}$	0	2	∞
Third order	13	$\dfrac{\Delta t^n}{\Delta t^{n+1}+2\Delta t^n}$	$\dfrac{(2\theta-1)\Delta t^{n+1}}{\Delta t^{n+1}+\Delta t^n}$	0	3	—
General	14	Equation (10b)	Equation (10a)	Equation (10c)	4	—

A unique set of θ and β exists when $\phi=0$, to make the scheme of order 3. Finally, a third condition has to be satisfied to obtain a fourth-order scheme:

$$\phi = -\frac{1}{2}\frac{(\Delta t^{n+1})^2}{(\Delta t^{n+1})^2+\Delta t^{n+1}\Delta t^n+(\Delta t^n)^2} \tag{10c}$$

In this case, the solution at the previous time step is needed in addition to the solution at t^n. Table I summarizes the principal configurations that can be obtained from Equation (9) also called the Beam–Warming [21] discretization. In this study, we will focus on the second-order time scheme.

In order to construct the implicit operator, the non-linear spatial operator $L(\mathbf{Q}^{n+1})$ needs to be linearized. Three approaches can be followed.

One step method: In a way, linearizing the spatial operator is making a first-order Taylor development, like:

$$L(\mathbf{Q}^{n+1}) = L(\mathbf{Q}^n) + \left.\frac{\partial L}{\partial \mathbf{Q}}\right|^n \Delta\mathbf{Q}^{n+1} + O(\Delta t^{n+1})$$

Substituting in Equation (9) leads to the following linear system:

$$\left[(1+\beta)\frac{I}{\Delta t^{n+1}} + \theta\frac{1}{J}\left.\frac{\partial L}{\partial \mathbf{Q}}\right|^n\right]\Delta\mathbf{Q}^{n+1} = \beta\frac{\Delta\mathbf{Q}^n}{\Delta t^n} - \frac{1}{J}(1+\phi)L(\mathbf{Q}^n) + \frac{1}{J}\phi L(\mathbf{Q}^{n-1}) \tag{11}$$

where I is the identity matrix. This scheme will be referred to as STEP. This method is usually applied when non-linearities are weak and can be resolved over a physical time step, or when a steady-state solution is sought.

Newton method: When an unsteady solution is calculated, it can be interesting to solve non-linearities by introducing subiterations between two physical time steps. A steady-state solution of the non-linear residual equation (11) is calculated:

$$\frac{1}{J}K(\mathbf{Q}^{n+1}) = (1+\beta)\frac{\Delta\mathbf{Q}^{n+1}}{\Delta t^{n+1}} - \beta\frac{\Delta\mathbf{Q}^n}{\Delta t^n} + \frac{1}{J}[\theta L(\mathbf{Q}^{n+1}) + (1-\theta+\phi)L(\mathbf{Q}^n) - \phi L(\mathbf{Q}^{n-1})]$$

The implicit Newton method consists of decreasing the non-linear residual $K(\mathbf{Q}^{n+1})$ at each time step and therefore to look for the following solution:

$$\frac{1}{J}K(\mathbf{Q}^{n+1})=0$$

An iterative Newton method is used, which writes:

$$\frac{1}{J}\frac{\partial K}{\partial \mathbf{Q}}\bigg|^{m}\Delta\mathbf{Q}^{n+1,m+1}=-\frac{1}{J}K(\mathbf{Q}^{n+1,m}) \tag{12}$$

where $\Delta\mathbf{Q}^{n+1,m+1}=\mathbf{Q}^{n+1,m+1}-\mathbf{Q}^{n+1,m}$ and m denotes the iteration number of the Newton method. Convergence is reached when $\Delta\mathbf{Q}^{n+1,m+1}=0$, or equivalently $\mathbf{Q}^{n+1,m+1}=\mathbf{Q}^{n+1}$. Equation (12) can be rewritten using a linear expansion of $K(\mathbf{Q}^{n+1,m+1})$:

$$\left[(1+\beta)\frac{I}{\Delta t^{n+1}}+\theta\frac{1}{J}\frac{\partial L}{\partial \mathbf{Q}}\bigg|^{n+1,m}\right]\Delta\mathbf{Q}^{n+1,m+1}=-\frac{1}{J}K(\mathbf{Q}^{n+1,m})$$

or again

$$\begin{aligned}\left[(1+\beta)\frac{I}{\Delta t^{n+1}}+\theta\frac{1}{J}\frac{\partial L}{\partial \mathbf{Q}}\bigg|^{n+1,m}\right]\Delta\mathbf{Q}^{n+1,m+1}&\\ =\beta\frac{\Delta\mathbf{Q}^{n}}{\Delta t^{n}}-\frac{1}{J}(1-\theta+\phi)L(\mathbf{Q}^{n})+\frac{1}{J}\phi L(\mathbf{Q}^{n-1})&\\ -(1+\beta)\frac{\mathbf{Q}^{n+1,m}-\mathbf{Q}^{n}}{\Delta t^{n+1}}-\frac{1}{J}\theta L(\mathbf{Q}^{n+1,m})&\end{aligned} \tag{13}$$

During Newton's iterations, the terms independent of m are fixed. This equation is formally very similar to the STEP method Equation (11), where only one subiteration is performed. This method will be referred to as NWT.

Dual time stepping method: Newton's approach is a particular case of dual time stepping where the non-linear residual is supposed to satisfy the following ordinary differential equation:

$$\frac{\mathrm{d}\mathbf{Q}}{\mathrm{d}t^{*}}=-\frac{1}{J}K(\mathbf{Q}) \tag{14}$$

The characteristic time t^{*} of this equation is independent of the physical time of the Euler equation (7). This dual time step can be chosen in order to accelerate the resolution of Equation (14), for example using a steady implicit scheme like the implicit Euler scheme:

$$\frac{\mathbf{Q}^{n+1,m+1}-\mathbf{Q}^{n+1,m}}{\Delta t^{*}}=-\frac{1}{J}K(\mathbf{Q}^{n+1,m+1})$$

Linearization of the right-hand side term can be performed in the same manner as in the former methods so that the equation becomes

$$\left[\frac{I}{\Delta t^{*}}+\frac{1}{J}\frac{\partial K}{\partial \mathbf{Q}}\bigg|^{n+1,m}\right]\Delta\mathbf{Q}^{n+1,m+1}=-\frac{1}{J}K(\mathbf{Q}^{n+1,m+1})$$

where again $\Delta\mathbf{Q}^{n+1,m+1} = \mathbf{Q}^{n+1,m+1} - \mathbf{Q}^{n+1,m}$ and m denotes the iteration number of the dual time stepping method. Further development of the Jacobian leads to

$$\left[\frac{I}{\Delta t^*} + (1+\beta)\frac{I}{\Delta t^{n+1}} + \theta\frac{1}{J}\frac{\partial L}{\partial \mathbf{Q}}\bigg|^{n+1,m}\right]\Delta\mathbf{Q}^{n+1,m+1} = -\frac{1}{J}K(\mathbf{Q}^{n+1,m+1})$$

or again

$$\begin{aligned}\left[\frac{I}{\Delta t^*} + (1+\beta)\frac{I}{\Delta t^{n+1}} + \theta\frac{1}{J}\frac{\partial L}{\partial \mathbf{Q}}\bigg|^{n+1,m}\right]\Delta\mathbf{Q}^{n+1,m+1} \\ = \beta\frac{\Delta\mathbf{Q}^n}{\Delta t^n} - \frac{1}{J}(1-\theta+\phi)L(\mathbf{Q}^n) + \frac{1}{J}\phi L(\mathbf{Q}^{n-1}) \\ -(1+\beta)\frac{(\mathbf{Q}^{n+1,m}-\mathbf{Q}^n)}{\Delta t^{n+1}} - \frac{1}{J}\theta L(\mathbf{Q}^{n+1,m})\end{aligned} \tag{15}$$

This method will be referred to as DUAL. Compared to the NWT approach, the dual time step allows dominant diagonal of the iterative matrix. Moreover, the Euler implicit scheme is unconditionally stable so that Δt^* can be freely chosen to accelerate the resolution of the non-linear term.

The discussed methods require evaluation of the Jacobian matrix of the spatial operator $L(\mathbf{Q})$. Its construction and the resolution of the matrix system is detailed in Section 3.4. At every point of the mesh, the spatial operator is written as

$$-\frac{1}{J_i}L(\mathbf{Q})|_i = -\frac{1}{J_i}[f_{i+1/2} - f_{i-1/2}] \tag{16}$$

so that the evaluation of the Jacobian matrix of $L(\mathbf{Q})$ is equivalent to the evaluation of the Jacobian matrix of convective fluxes schemes $f_{i+1/2}(\mathbf{Q})$. The dependency of the spatial scheme clearly appears through

$$-\frac{1}{J}\frac{\partial L}{\partial \mathbf{Q}}\bigg|^{n+1,m}\Delta\mathbf{Q}^{n+1,m+1} = -\frac{1}{J}\left[\frac{\partial f_{i+1/2}}{\partial \mathbf{Q}}\bigg|^{n+1,m} - \frac{\partial f_{i-1/2}}{\partial \mathbf{Q}}\bigg|^{n+1,m}\right]\Delta\mathbf{Q}^{n+1,m+1}$$

The explicit expression of TVD and WENO schemes retained in this study are presented in the next section.

3.3. Spatial discretization

The Jacobian matrix $A = \partial\mathbf{F}/\partial\mathbf{Q}$ of the convective flux $\mathbf{F}$ of the conservative system (1) is defined in physical space as

$$A = \begin{pmatrix} 0 & 1 & 0 \\ -u^2 + \dfrac{\gamma-1}{2}\vec{u}^2 & (3-\gamma)u & \gamma-1 \\ -u[\gamma e - (\gamma-1)\vec{u}^2] & \gamma e - \dfrac{\gamma-1}{2}(\vec{u}^2+2u^2) & \gamma u \end{pmatrix} \tag{17}$$

The eigenvalue matrix of A may be defined as

$$\Lambda = \begin{pmatrix} \vec{u}.\vec{n} & 0 & 0 \\ 0 & \vec{u}.\vec{n} + c & 0 \\ 0 & 0 & \vec{u}.\vec{n} - c \end{pmatrix}$$

where $\vec{n}$ is an arbitrary spatial direction and c the speed of sound. These eigenvalues represent the propagation velocity of waves in the hyperbolic differential system. In the one-dimensional approximation $\vec{n}$ may be defined in the direction of the flow velocity $\vec{u}$. The left eigenvectors matrix R^{-1}, such that $\Lambda = R^{-1}AR$, is given by

$$R^{-1} = \begin{pmatrix} c^3 - \frac{1}{2}(\gamma-1)\vec{u}^2 & (\gamma-1)u & -(\gamma-1) \\ \frac{1}{2}\left[\frac{1}{2}(\gamma-1)\vec{u}^2 - \vec{u}.\vec{n}c\right] & -\frac{1}{2}[(\gamma-1)u - cn_x] & \frac{1}{2}(\gamma-1) \\ \frac{1}{2}\left[\frac{1}{2}(\gamma-1)\vec{u}^2 + \vec{u}.\vec{n}c\right] & -\frac{1}{2}[(\gamma-1)u + cn_x] & \frac{1}{2}(\gamma-1) \end{pmatrix}$$

The right eigenvector matrix related to the conservative variables is then

$$R = \begin{pmatrix} \frac{1}{c^2} & \frac{1}{c^2} & \frac{1}{c^2} \\ \frac{u}{c^2} & \frac{1}{c^2}[u + cn_x] & \frac{1}{c^2}[u - c] \\ \frac{1}{2}\frac{\vec{u}^2}{c^2} & \frac{1}{c^2}[h_T + c\vec{u}.\vec{n}] & \frac{1}{c^2}[h_T = c\vec{u}.\vec{n}] \end{pmatrix}$$

where $h_T = \frac{1}{2}\vec{u}^2 + c^2/(\gamma-1)$ is the total enthalpy. The information propagating along these waves is described by the characteristic variables α, obtained by the projection of the increments of the conservative variables $\delta\mathbf{Q}$ on the characteristic lines using the left eigenvectors matrix R^{-1}:

$$\alpha = R^{-1}\delta\mathbf{Q}$$

In the spatial discretizations described hereafter, left and right eigenvectors are evaluated at the cell interface $i + 1/2$. Values of physical quantities at this location are then estimated by the Roe average [22], defined as

$$\rho_{i+1/2} = \sqrt{\rho_i \rho_{i+1}} \tag{18a}$$

$$u_{i+1/2} = \frac{u_i\sqrt{\rho_{i+1}} + u_{i+1}\sqrt{\rho_i}}{\sqrt{\rho_{i+1}} + \sqrt{\rho_i}} \tag{18b}$$

$$h_{i+1/2} = \frac{h_i\sqrt{\rho_{i+1}} + h_{i+1}\sqrt{\rho_i}}{\sqrt{\rho_{i+1}} + \sqrt{\rho_i}} \tag{18c}$$

In particular, the TVD and WENO scheme presented here are based on a Roe formulation.

3.3.1. TVD scheme. Harten–Yee's shock capturing scheme [2, 10, 23, 24] is a second-order TVD scheme. The convective flux at the cell interface $i+\frac{1}{2}$ is decomposed in physical space as

$$F_{i+1/2} = \frac{1}{2}[F_{i+1} + F_i - R_{i+1/2}\phi_{i+1/2}]$$

where $R_{i+1/2}$ denotes the right eigenvector matrix of the Jacobian matrix A at the cell interface evaluated using the Roe formula (18a). In the computational domain, the contravariant flux components for the one-dimensional system are then given by

$$f_{i+1/2} = \frac{1}{2}[b_1^1|_{1+1/2}(F_{i+1} + F_i) - \mathscr{R}_{i+1/2}\phi_{i+1/2}] \tag{19}$$

where $\mathscr{R}_{i+1/2}$ denotes to the right eigenvector matrix of the Jacobian matrix $\mathscr{A}$, the projection of A in the computational domain:

$$\mathscr{A} = b_1^1 A$$

In physical space, the vector $\phi_{i+1/2}$ is defined as

$$\phi_{i+1/2} = -\sigma(\lambda_{i+1/2})(g_{i+1} + g_i) + \psi(\lambda_{i+1/2} + \gamma_{i+1/2})\alpha_{i+1/2} \tag{20}$$

where $\alpha_{i+1/2}$ represents the characteristic increment at the cell interface, calculated from

$$\alpha_{i+1/2} = R_{i+1/2}^{-1}(\mathbf{Q}_{i+1} - \mathbf{Q}_i)$$

The function ψ is defined by

$$\psi(z) = \begin{cases} |z| & \text{if } |z| \geqslant \varepsilon \\ \dfrac{1}{2}\left(\dfrac{z^2}{\varepsilon} + \varepsilon\right) & \text{if } |z| < \varepsilon \end{cases}$$

This function provides an entropy correction in the presence of acoustic waves. The value of ε can be estimated as the fraction χ of the spectral radius of A, like $\varepsilon = \chi r(A)$. The correction $\gamma_{i+1/2}$ on the eigenvalues $\lambda_{i+1/2}$ in Equation (20) is defined as

$$\gamma_{i+1/2} = \begin{cases} \sigma(\lambda_{i+1/2})\dfrac{(g_{i+1} - g_i)}{\alpha_{i+1/2}} & \text{if } \alpha_{i+1/2} \neq 0 \\ 0 & \text{if } \alpha_{i+1/2} = 0 \end{cases}$$

where σ is given by

$$\sigma(z) = \frac{1}{2}\left(\psi(z) - \varpi\frac{\Delta t}{J}z^2\right)$$

When first-order time scheme is used, this function renders the scheme globally of second order [25]. For unsteady problems, however, it is preferable to set to $\varpi = 0$ so that the function becomes independent of time. The limiter g used in this study is the Van Leer function, defined as

$$g_i = \begin{cases} \dfrac{\alpha_{i+1/2}\alpha_{i-1/2} + |\alpha_{i+1/2}\alpha_{i-1/2}|}{(\alpha_{i+1/2} + \alpha_{i-1/2})} & \text{if } \alpha_{i+1/2} + \alpha_{i-1/2} \neq 0 \\ 0 & \text{if } \alpha_{i+1/2} + \alpha_{i-1/2} = 0 \end{cases}$$

The influence of the parameters χ and ϖ has been studied in Reference [26]. The scheme retained in this study uses $\chi = 0$ and $\varpi = 0$ and will be referred to as TVD.

3.3.2. WENO scheme. The WENO approach retained in this study [15] is applied to the contravariant components of the convective fluxes. In order to take into account the hyperbolic character of the system, fluxes evaluated at the mesh points are first projected onto characteristic lines using the left eigenvector matrix $R^{-1}_{i+1/2}$:

$$\bar{\mathbf{f}}_i = R^{-1}_{i+1/2}\mathbf{f}_i$$

where $R^{-1}_{i+1/2}$ is evaluated at the cell interface using the Roe averaging formula (18a)–(18c). The WENO reconstruction is then applied to the projected fluxes $\bar{\mathbf{f}}_i$. The reconstruction of the flux is upwinded at the interface $i+\frac{1}{2}$ according to incoming or outgoing characteristics, or equivalently, to the sign of the eigenvalues of Jacobian matrix at the interface. More precisely,

$$\text{if } \lambda^k_{i+1/2} \geqslant 0 \quad \text{then} \quad \bar{f}^k_{i+1/2} = \bar{f}^{k+}_{i+1/2}$$

$$\text{if } \lambda^k_{i+1/2} < 0 \quad \text{then} \quad \bar{f}^k_{i+1/2} = \bar{f}^{k-}_{i+1/2}$$

where $\bar{f}^k_{i+1/2}$ denotes the kth component of the flux vector. The fluxes $\bar{\mathbf{f}}^+_{i+1/2}$ and $\bar{\mathbf{f}}^-_{i+1/2}$ are the WENO fluxes reconstructed from $\bar{\mathbf{f}}_i$ on stencils which are shifted in, respectively, the left and right direction with respect to the interface $i+\frac{1}{2}$, as is detailed below. After reconstruction, the flux $\mathbf{f}_{i+1/2}$ is transformed back to physical space using the right eigenvector matrix $R_{i+1/2}$

$$\mathbf{f}_{i+1/2} = R_{i+1/2}\bar{\mathbf{f}}_{i+1/2}$$

Since the WENO reconstruction is equivalent for each component $\bar{\mathbf{f}}^k_{i+1/2}$ of the flux vector, the index k is omitted in the following to simplify the notation.

The reconstruction of $\bar{f}^+_{i+1/2}$ is performed from k candidate stencils:

$$S_r(i) = \{\xi_{i-r}, \ldots, \xi_{i-r+k-1}\} \text{ with } r = 0, \ldots, k-1$$

The candidate stencils for $k = 3$ are represented in Figure 3. On each stencil $S_r(i)$ a $k-1$ order polynomial interpolation can be built such that:

$$\bar{f}^{r-}_{i+1/2} = \sum_{n=0}^{k-1} c_{n,r+1}\bar{f}_{i+n+1+r+1-k}$$

$$\bar{f}^{r+}_{i+1/2} = \sum_{n=0}^{k-1} c_{n,r}\bar{f}_{i+n+1+r-k} \text{ with } r = 0, \ldots, k-1$$

The weight coefficients $c_{n,r}$ where $n = 0, \ldots, k-1$ and $r = 0, \ldots, k$, for uniform meshes are listed in Table II. The WENO reconstruction is a convex combination of all the candidate interpolations $\bar{f}^r_{i+1/2}$, and writes:

$$\bar{f}^-_{i+1/2} = \sum_{r=0}^{k-1} \omega^-_r \bar{f}^{r-}_{i+1/2}$$

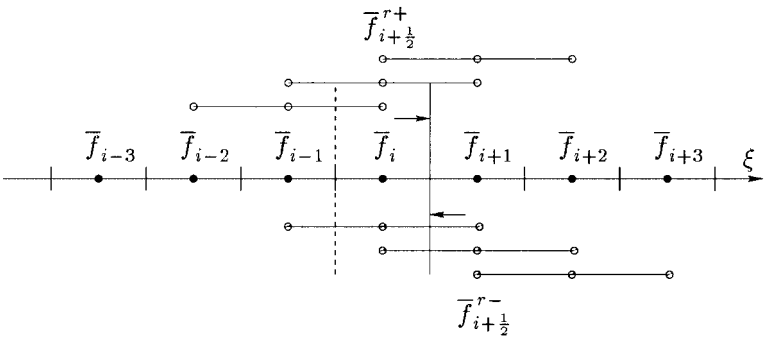

Figure 3. Candidate stencils for the left ($\lambda_{i+1/2} \geqslant 0$) and right ($\lambda_{i+1/2} < 0$) WENO reconstructions at the cell interface $i + \frac{1}{2}$ for $k = 3$.

Table II. Values of $c(n,r)$ for $k = 2$ and 3.

k	r	$n=0$	$n=1$	$n=2$
2	0	$-1/2$	3/2	
	1	1/2	1/2	
	2	3/2	$-1/2$	
3	0	1/3	$-7/6$	11/6
	1	$-1/6$	5/6	1/3
	2	1/3	5/6	$-$ 1/6
	3	11/6	$-7/6$	1/3

$$\bar{f}^{+}_{i+1/2} = \sum_{r=0}^{k-1} \omega^{+}_{r} \bar{f}^{r+}_{i+1/2}$$

where

$$\omega^{\pm}_{r} = \frac{\alpha^{\pm}_{r}}{\sum_{n=0}^{k-1} \alpha^{\pm}_{n}} \text{ with } \alpha^{\pm}_{r} = \frac{d^{\pm}_{r}}{(\varepsilon + \beta^{\pm}_{r}(i))^2}$$

The constant $\varepsilon = 10^{-6}$ prevents the denominator to become zero [27]. The functions $\beta^{\pm}_{r}(i)$ are regularity indicators of the stencil $S_r(i)$, placing the weight on the smoothest stencils. They are calculated by divided differences. For $k = 2$ the divided differences are:

$$\beta^{+}_{0}(i) = (\bar{f}_i - \bar{f}_{i-1})^2$$

$$\beta^{+}_{1}(i) = (\bar{f}_{i+1} - \bar{f}_i)^2$$

$$\beta^{-}_{0}(i) = (\bar{f}_{i+1} - \bar{f}_i)^2$$

$$\beta^{-}_{1}(i) = (\bar{f}_{i+2} - \bar{f}_{i+1})^2$$

Table III. Values of d_r^+ for $k=2$ and 3.

k	$n=0$	$n=1$	$n=2$
2	1/3	2/3	
3	1/10	6/10	3/10

Table IV. Values of d_r^- for $k=2$ and 3.

k	$n=0$	$n=1$	$n=2$
2	2/3	1/3	
3	3/10	6/10	1/10

For $k=3$, Jiang and Shu [15] proposed the following approximation:

$$\beta_0^+(i)=\frac{13}{12}(\bar{f}_{i-2}-2\bar{f}_{i-1}+\bar{f}_i)^2+\frac{1}{4}(\bar{f}_{i-2}-4\bar{f}_{i-1}+3\bar{f}_i)^2$$

$$\beta_1^+(i)=\frac{13}{12}(\bar{f}_{i-1}-2\bar{f}_i+\bar{f}_{i+1})^2+\frac{1}{4}(\bar{f}_{i-1}-\bar{f}_{i+1})^2$$

$$\beta_2^+(i)=\frac{13}{12}(\bar{f}_i-2\bar{f}_{i+1}+\bar{f}_{i+2})^2+\frac{1}{4}(3\bar{f}_i-4\bar{f}_{i+1}+\bar{f}_{i+2})^2$$

$$\beta_0^-(i)=\frac{13}{12}(\bar{f}_{i-1}-2\bar{f}_i+\bar{f}_{i+1})^2+\frac{1}{4}(\bar{f}_{i-1}-4\bar{f}_i+3\bar{f}_{i+1})^2$$

$$\beta_1^-(i)=\frac{13}{12}(\bar{f}_i-2\bar{f}_{i+1}+\bar{f}_{i+2})^2+\frac{1}{4}(\bar{f}_i-\bar{f}_{i+2})^2$$

$$\beta_2^-(i)=\frac{13}{12}(\bar{f}_{i+1}-2\bar{f}_{i+2}+\bar{f}_{i+3})^2+\frac{1}{4}(3\bar{f}_i-4\bar{f}_{i+1}+\bar{f}_{i+2})^2$$

The $d_r^\pm$ coefficients are chosen to render the scheme $2k-1$ order on smooth meshes. Their values for $k=2$ and 3 are given in Tables III and IV. Note that:

$$d_r^-=d_{k-1-r}^+$$

$$\beta_r^-(i)=\beta_r^+(i+1)$$

For $k=3$, the WENO scheme retained in this study, a space resolution of order $2k-1=5$ is obtained on smooth solutions.

Scheme	k	order
WENO	3	5

3.4. Construction of implicit operator

The resolution of the implicit schemes requires the linearization of the implicit spatial operator and subsequently the inversion of the resulting system. They are detailed below for, respectively, the TVD schemes and the WENO scheme.

3.4.1. TVD schemes. As described in the previous section, the contravariant flux is written as

$$f_{i+1/2} = \frac{1}{2}[b_1^1|_{i+1/2}(F_{i+1} + F_i) - R_{i+1/2}\phi_{i+1/2}]$$

with

$$\phi_{i+1/2} = -\sigma(\lambda_{i+1/2})(g_{i+1} + g_i) + \psi(\lambda_{i+1/2} + \gamma_{i+1/2})\alpha_{i+1/2}$$

and

$$\alpha_{i+1/2} = R_{i+1/2}^{-1}(\mathbf{Q}_{i+1} - \mathbf{Q}_i)$$

or equivalently:

$$\phi_{i+1/2} = \begin{cases} \left[-\sigma(\lambda_{i+1/2})\dfrac{(g_{i+1} + g_i)}{\alpha_{i+1/2}} + \psi(\lambda_{i+1/2} + \gamma_{i+1/2})\right]\alpha_{i+1/2} & \text{if } \alpha_{i+1/2} \neq 0 \\ 0 & \text{if } \alpha_{i+1/2} = 0 \end{cases}$$

Linearization of the implicit operator: For unsteady problems, the linearization of the implicit fluxes has to respect a conservative form in space and time. This is the case when

$$\frac{1}{J}\frac{\partial f_{i+1/2}}{\partial \mathbf{Q}}\bigg|^{n+1,m} \Delta\mathbf{Q}^{n+1,m+1} = \frac{1}{2}[{}^{\xi}a_{i+1}^{n+1,m}\Delta\mathbf{Q}_{i+1}^{n+1,m+1} + {}^{\xi}a_i^{n+1,m}\Delta\mathbf{Q}_i^{n+1,m+1} - R_{i+1/2}\phi'_{i+1/2}R_{i+1/2}^{-1}(\Delta\mathbf{Q}_{i+1}^{n+1,m+1} - \Delta\mathbf{Q}_i^{n+1,m+1})] \tag{21}$$

where all the elements are calculated in the computational domain, in particular ${}^{\xi}a, R$ and R^{-1} and

$$\phi'_{i+1/2} = \begin{cases} -\dfrac{(g_{i+1} + g_i)}{\alpha_{i+1/2}} + \psi(\lambda_{i+1/2} + \gamma_{i+1/2}) & \text{if } \alpha_{i+1/2} \neq 0 \\ 0 & \text{if } \alpha_{i+1/2} = 0 \end{cases}$$

The Jacobian at the cell boundary $i + \frac{1}{2}$ involves the known neighbouring points i and $i + 1$, so that a three points scheme is obtained. With $\Omega = R\phi' R^{-1}$ the implicit spatial operator can be written as a tridiagonal block matrix:

$$\frac{1}{J}\frac{\partial L}{\partial \mathbf{Q}}\bigg|^{n+1,m} \Delta\mathbf{Q}^{n+1,m+1} = c_M\Delta\mathbf{Q}_{i-1}^{n+1,m+1} + c_N\Delta\mathbf{Q}_i^{n+1,m+1} + c_P\Delta\mathbf{Q}_{i+1}^{n+1,m+1} \tag{22}$$

where coefficients c_M, c_N and c_P are 3×3 matrices depending on values at i. They are defined as

$$c_M = \frac{1}{2}[-{}^{\xi}a_{i-1}^{n+1,m} - \Omega_{i-1/2}^{n+1,m}] \tag{23a}$$

$$c_N = \frac{1}{2}[\Omega_{i+1/2}^{n+1,m} + \Omega_{i-1/2}^{n+1,m}] \tag{23b}$$

$$c_P = \frac{1}{2}[{}^{\xi}a_{i+1}^{n+1,m} - \Omega_{i+1/2}^{n+1,m}] \tag{23c}$$

In this case, the discrete equations can be written schematically as

$$C_M \Delta\mathbf{Q}_{i-1}^{n+1,m+1} + C_N \Delta\mathbf{Q}_{i}^{n+1,m+1} + C_P \Delta\mathbf{Q}_{i+1}^{n+1,m+1} = C_S \tag{24}$$

where only the source and the diagonal terms are modified, depending on the time scheme used. For dual time stepping, they are defined as

$$\begin{aligned}
C_M &= \theta c_M \\
C_N &= \theta c_N + \frac{I}{\Delta t^*} + (1+\beta)\frac{1}{\Delta t^{n+1}} \\
C_P &= \theta c_P \\
C_S &= \beta \frac{\Delta\mathbf{Q}^n}{\Delta t^n} - \frac{1}{J}(1-\theta+\phi)L(\mathbf{Q}^n) + \frac{1}{J}\phi L(\mathbf{Q}^{n-1}) \\
&\quad -(1+\beta)\frac{(\mathbf{Q}^{n+1,m} - \mathbf{Q}^n)}{\Delta t^{n+1}} - \frac{1}{J}\theta L(\mathbf{Q}^{n+1,m})
\end{aligned}$$

System inversion: The Harten–Yee TVD scheme uses a discrete stencil of three points in each spatial direction. The formation of the implicit operators therefore leads to a block tridiagonal matrix. In the one-dimensional case considered here these blocks are 3×3 and the matrix has the following form:

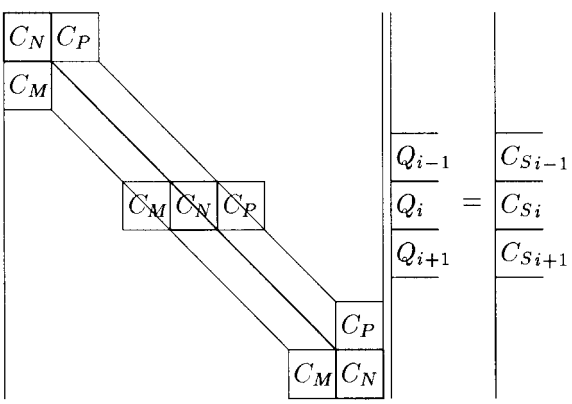

This matrix is inverted by incomplete LU (ILU) decomposition. For a tridiagonal matrix, this decomposition is exact. The system to invert can be written in the form

$$CX = b$$

Given the following decomposition

$$C = L_C + D_C + U_C$$

where L_C, U_C and D_C are, respectively, the lower, upper and diagonal bands of the C matrix, the decomposition consists of approaching C by M such that

$$M = LDU$$

where

$$L = L_C + D^{-1} \quad \text{and} \quad U = D^{-1} + U_C$$

leading to

$$M = L_C + (D^{-1} + L_C D U_C) + U_C$$

Identifying M to C gives an expression for D:

$$D^{-1} = D_C - L_C D U_C$$

which is easily solved since D is a diagonal matrix. The inversion of the 3×3 blocks of D is performed by a complete LU decomposition. Once D is calculated, the entire system is inverted by solving the respective lower and upper systems:

$$LY = b \quad \text{or} \quad Y = D(b - L_C Y)$$

$$DUX = Y \quad X = Y - DU_C X$$

3.4.2. WENO scheme. The convective scheme is written in the computational domain as:

$$f_{i+1/2} = R_{i+1/2} \bar{f}_{i+1/2}$$

where

$$\bar{f}_{i+1/2} = \begin{cases} \bar{f}^{+}_{i+1/2} = \sum_{r=0}^{k-1} \omega_r^{+} \sum_{n=0}^{k-1} c_{n,r} \bar{f}_{i+n+1+r-k} & \text{if } \lambda_{i+1/2} \geqslant 0 \\ \bar{f}^{-}_{i+1/2} = \sum_{r=0}^{k-1} \omega_r^{-} \sum_{n=0}^{k-1} c_{n,r+1} \bar{f}_{i+n+1+r+1-k} & \text{if } \lambda_{i+1/2} < 0 \end{cases} \tag{25}$$

with $\bar{f}_i = R^{-1}_{i+1/2} f_i$. The sign of the eigenvalues can change from one flux component to another so that this test needs to be carried out for each flux component.

Linearization of the implicit operator: The preceding test can be written in a more schematic way using the sign function, defined by

$$\text{sign}(p) = 1 \quad \text{if } \Lambda_{i+1/2}(p) \geqslant 0$$

$$\text{sign}(p) = 0 \quad \text{if } \Lambda_{i+1/2}(p) < 0$$

Inserting this function and the previous expression for the projected flux in Equation (25) leads to:

$$\bar{f}_{i+1/2}(p) = \sum_{r=0}^{k-1}\sum_{n=0}^{k-1}[\mathrm{sign}(p)\omega_r^+(p)c_{n,r}R^{-1}_{i+n+1+r-k}(p,q)f_{i+n+1+r-k}(q)$$

$$+(1-\mathrm{sign}(p))\omega_r^-(p)c_{n,r+1}R^{-1}_{i+n+1+r+1-k}(p,q)f_{i+n+1+r+1-k}(q)]$$

The calculation of the Jacobian can be carried out in a simple manner using the Jacobian matrix of the convective fluxes in calculation space. The divergence operator is given by

$$\frac{\partial F^i}{\partial X^i} = \frac{1}{J}\frac{\partial f^i}{\partial \xi^i}$$

so that denoting the Jacobian matrix in, respectively, the physical and computational domain by

$$A^i \equiv \frac{\partial F^i}{\partial \mathbf{Q}} \quad \text{and} \quad a^i \equiv \frac{\partial f^i}{\partial \mathbf{Q}}$$

we obtain

$$a^i = J\frac{\partial \xi^i}{\partial X^j}A^j$$

or

$$\frac{1}{J}\frac{\partial f^i}{\partial \mathbf{Q}} = \frac{\partial \xi^i}{\partial X^j}\frac{\partial F^j}{\partial \mathbf{Q}}$$

This can be written as

$${}^{\xi}a^i \equiv \frac{1}{J}a^i = \frac{\partial \xi^i}{\partial X^j}A^j$$

In the one-dimensional case, there is only one flux component in the ξ direction and setting $f \equiv f^1$ gives

$${}^{\xi}a \equiv \frac{1}{J}a = \frac{\partial \xi}{\partial X}A$$

If we consider the cell interface value of the flux projected on the left eigenvector matrix R^{-1}, we obtain:

$$\frac{1}{J}\frac{\partial f_{i+1/2}}{\partial \mathbf{Q}} = R_{i+1/2}\left[\frac{1}{J}\frac{\partial \bar{f}_{i+1/2}}{\partial \mathbf{Q}}\right]$$

and

$$\frac{1}{J}\frac{\partial \bar{f}_{i+1/2}}{\partial Q}(p,q) = \sum_{r=0}^{k-1}\sum_{n=0}^{k-1}\left[\mathrm{sign}(p)\omega_r^+(p)c_{n,r}R^{-1}_{i+n+1+r-k}(p,r)\frac{1}{J}\frac{\partial f_{i+n+1+r-k}}{\partial Q}(r,q)\right.$$

$$\left.+(1-\mathrm{sign}(p))\omega_r^-(p)c_{n,r+1}R^{-1}_{i+n+1+r+1-k}(p,r)\frac{1}{J}\frac{\partial f_{i+n+1+r+1-k}}{\partial Q}(r,q)\right]$$

so that,

$$\frac{1}{J}\frac{\partial \bar{f}_{i+1/2}}{\partial Q}(p,q) = \sum_{r=0}^{k-1}\sum_{n=0}^{k-1}[\mathrm{sign}(p)\omega_r^+(p)c_{n,r}R^{-1}_{i+n+1+r-k}(p,r)^{\xi}a_{i+n+1+r-k}(r,q) + (1-\mathrm{sign}(p))\omega_r^-(p)c_{n,r+1}R^{-1}_{i+n+1+r+1-k}(p,r)^{\xi}a_{i+n+1+r+1-k}(r,q)]$$

The reconstruction on the cell interface requires $2k$ points, leading to a special discretization expanding over $2k+1$ points.

System inversion: The WENO scheme with $k=3$ covers a discrete stencil of 7 points in each spatial direction. The implicit operator therefore forms a 3×3 block heptadiagonal matrix with the following structure:

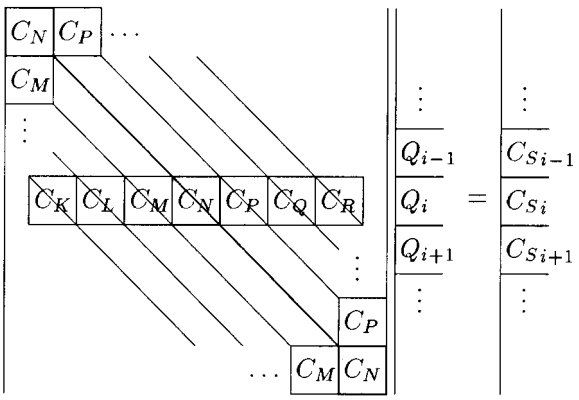

This system is inverted by an incomplete LU decomposition. The system to solve is written as

$$CX = b$$

and we look for the LU decomposition of the form

$$M = LDU$$

where

$$L = L_C + D^{-1} \quad \text{and} \quad U = D^{-1} + U_C$$

Again, the diagonal matrix D is calculated from:

$$D^{-1} = D_C - L_C D U_C$$

In contrast to the previous case, this decomposition is not exact and the matrix M approaches C with a residual r defined by

$$C = M - r$$

Table V. Initial conditions of the shock tube test cases.

Case	Domain	Final time	ρ_L	u_L	e_L	ρ_R	u_R	e_R
Sod	$[-5,5]$	2.00	1.0	0	2.5	0.125	0	2.0
Lax	$[-5,5]$	1.30	0.445	0.698	20.06	0.5	0	2.855

The residual must go to zero for the decomposition to obtain the best approximation of the matrix. This can be obtained by an iterative way by solving the system:

$$M(X^{q+1} - X^q) = b - CX^q$$

For large numbers of iterations, the solution X^{q+1} converges to the exact solution X.

If the construction of the implicit operator follows the approach usually retained for TVD schemes, this iterative resolution is no longer a necessity, since only the first three block diagonals are treated implicitly. In the implicit operator presented here the full set of candidate stencil is taken into account. This motivates the study of unsteady flows where sharp discontinuities are propagating.

4. NUMERICAL RESULTS

In this section, this implicit WENO scheme is tested against the TVD and explicit schemes in the case of two well-known problems: the one-dimensional shock tube and the shock-entropy wave interaction.

4.1. 1D shock tube

The one-dimensional shock tube is a typical Riemann problem used for testing numerical schemes for Euler equations of gas dynamics. The system is calculated from the initial condition:

$$(\rho, u, e) = \begin{cases} (\rho_L, u_L, e_L), & x < 0 \\ (\rho_R, u_R, e_R), & x > 0 \end{cases}$$

so that the initial shock is located at $x = 0$. Two classical cases defined by Sod [28] and Lax [29] are calculated here. The initial conditions of these cases are recalled in Table V. Calculations are performed up to the indicated final time and compared to the exact solutions obtained in [6] from the application of Rankine–Hugoniot relations.

Sod's explicit solver: The results obtained with the explicit TVD and WENO scheme are shown in Figure 4. They are computed with CFL $= 0.5$ on a uniform grid of $i_m = 50$ points. Both solutions are very similar. Slight differences are nonetheless observed on the density profiles, where the WENO scheme appears to better capture the shock and the contact discontinuity than the TVD scheme. However, on the entropy evolution, oscillations in the expansion wave can be seen on the WENO solution that are absent for the TVD scheme. This may be attributed to the chosen reconstruction of the characteristic variables, as was suggested in Reference [27]. Testing different WENO reconstructions is however out of the

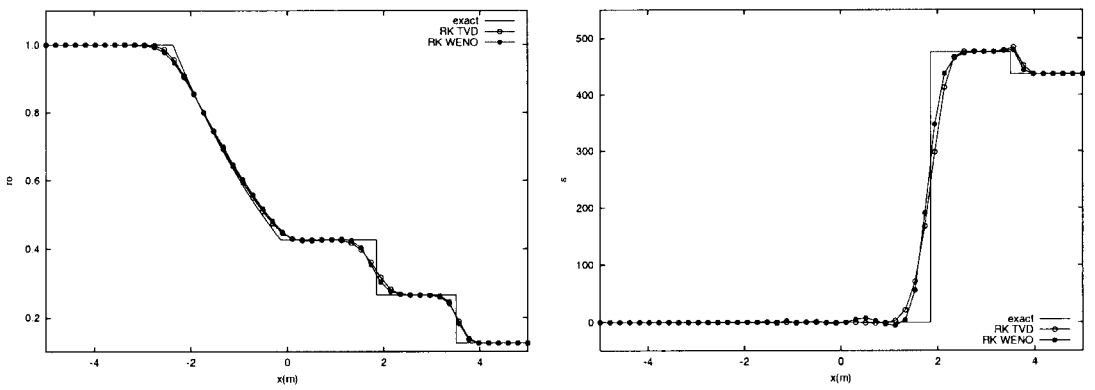

Figure 4. Numerical solution of Sod's problem with the explicit Runge–Kutta time scheme and the TVD and WENO spatial schemes for $N = 50$ and CFL $= 0.5$.

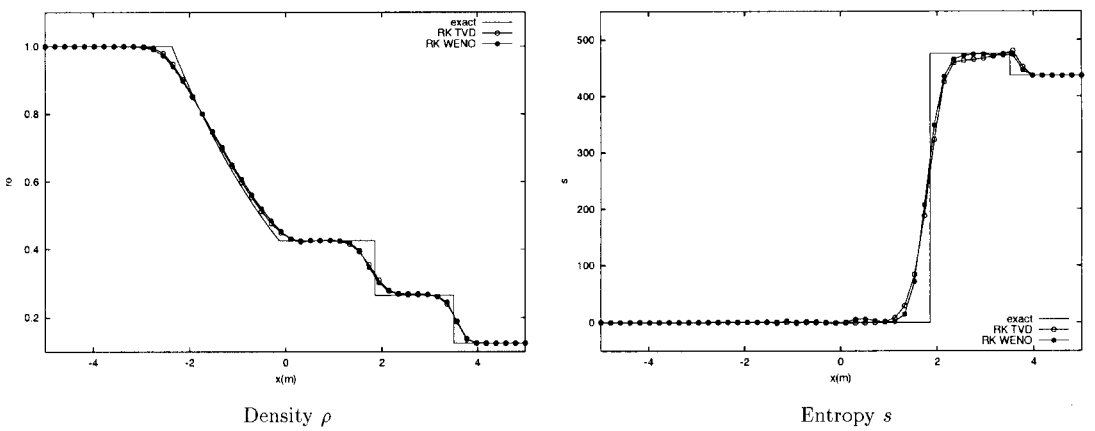

Figure 5. Numerical solution of Sod's problem with the explicit Runge–Kutta time scheme and the TVD and WENO spatial schemes for $N = 50$ and CFL $= 1.0$.

scope of this study, which focuses on the implicit solver. The explicit results will be taken as a reference to evaluate the performance of the implicit schemes.

Figure 5 shows the results for a CFL number of 1.0. The differences between the TVD and WENO schemes are now more pronounced. As in the previous case, there is no influence of the entropy correction on the TVD scheme results. The oscillations observed in the WENO scheme leads to an overestimation of the velocity at the end of the expansion wave. A better prediction of the shock wave is nonetheless observed on the entropy evolution with the WENO scheme.

Sod's implicit solver: Results of Sod's problem obtained with the implicit time schemes T, ER and I3 are presented in Figure 6 for CFL $= 0.5$ and in Figure 7 for CFL $= 1.0$. They are compared to the results obtained with the STEP method also shown in the figures.

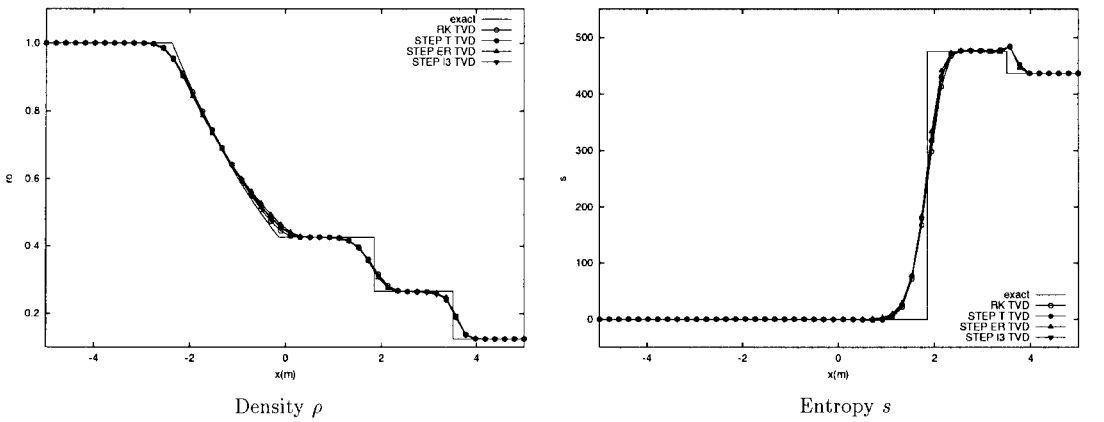

Figure 6. Numerical solution of Sod's problem with the STEP method and the TVD spatial scheme. Comparison of the explicit RK and implicit T, ER and I3 time schemes for $N = 50$ and CFL $= 0.5$.

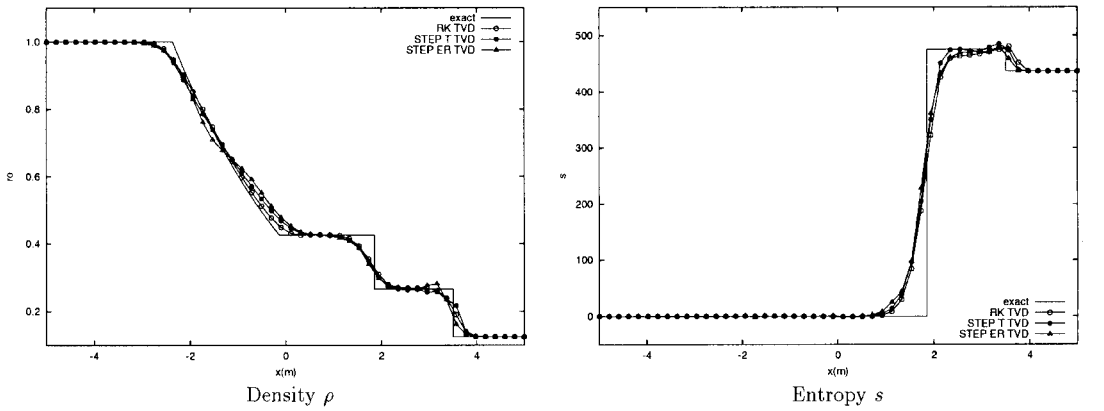

Figure 7. Numerical solution of Sod's problem with the STEP method and the TVD spatial scheme. Comparison of the explicit RK and implicit T and ER time schemes for $N = 50$ and CFL $= 1.0$.

The results obtained with the ER and I3 time schemes are very similar to those obtained with the T scheme for a CFL $= 0.5$. The second-order linearization performed to build the implicit operator allows working with a second-order time scheme at a moderate CFL number.

At a CFL number of 1.0, oscillations can be observed in the results obtained with the T time scheme. More severe oscillations are produced by the ER schemes while I3, not shown in the figure, becomes unstable. This might be due to the high frequency dispersive error of this scheme. Consequently, the T time scheme is preferred in this case. A better resolution of the non-linearities using the NWT or DUAL approach improves the resolution of the discontinuities as shown in Figures 8 and 9. The ER scheme is again unstable and lead to strong oscillations of the velocity in the vicinity of the shock. T and I3 exhibits better behaviour with the NWT method than with the STEP one. Globally, the DUAL approach

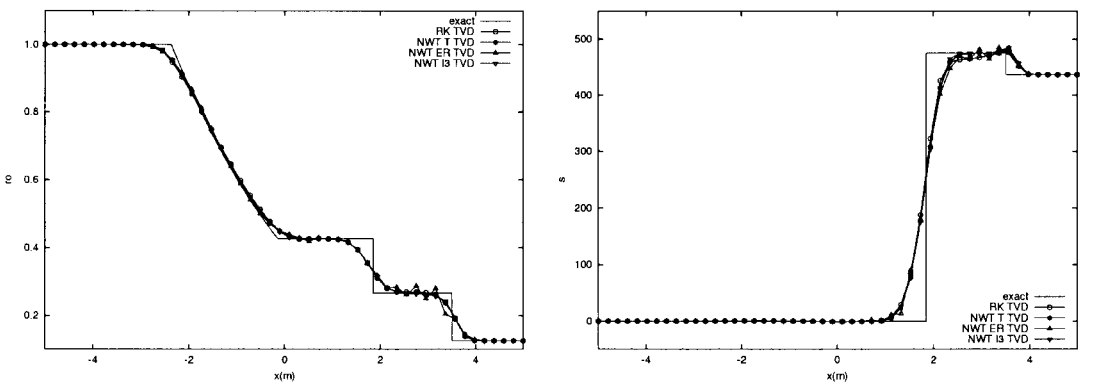

Figure 8. Numerical solution of Sod's problem with the NWT method and the TVD spatial scheme. Comparison of the explicit RK and implicit T and ER time schemes for $N = 50$ and CFL $= 1.0$.

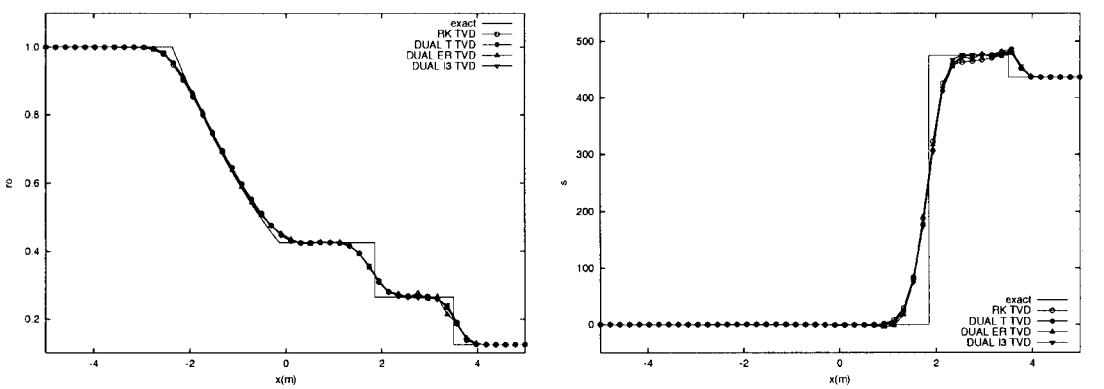

Figure 9. Numerical solution of Sod's problem with the DUAL method and the TVD spatial scheme. Comparison of the explicit RK and implicit T and ER time schemes for $N = 50$ and CFL $= 1.0$.

improves the solutions for every time scheme. Best results are obtained with the T time scheme and the DUAL approach.

Similar comments can be made when the WENO scheme is applied. The results obtained with the DUAL method are better than the other implicit schemes and the T and I3 time schemes give better results than the ER one (Figure 10).

The matrix associated with the fifth-order WENO scheme is heptadiagonal so that the ILU decomposition has to be solved with an iterative method. If only the first three block diagonals are resolved implicitly, this iterative approach is no longer a necessity. This approximation of the implicit WENO scheme, referred to as WE3C, is also computed and the results are shown in Figure 11. This scheme appears not well suited for unsteady solution with a shock, since the shock velocity is not accurately predicted.

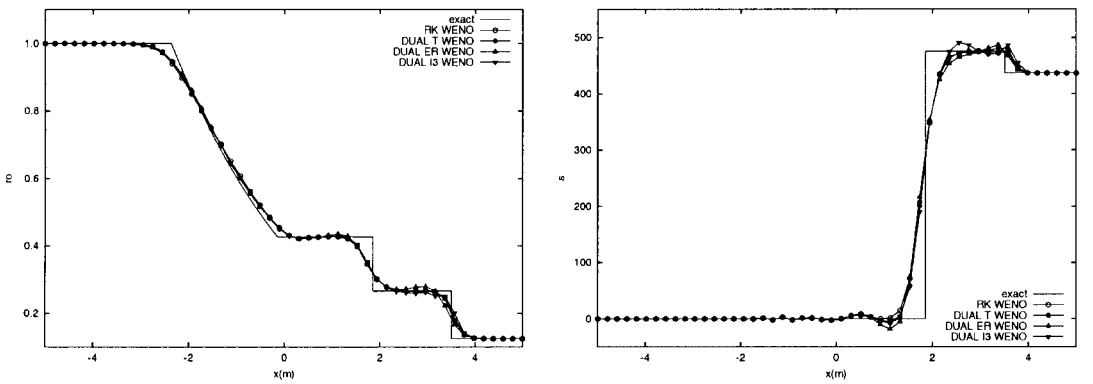

Density ρ Entropy s

Figure 10. Numerical solution of Sod's problem with the DUAL method and the WENO convective scheme. Comparison of the explicit RK and implicit T and ER time schemes for $N = 50$ and CFL $= 1.0$.

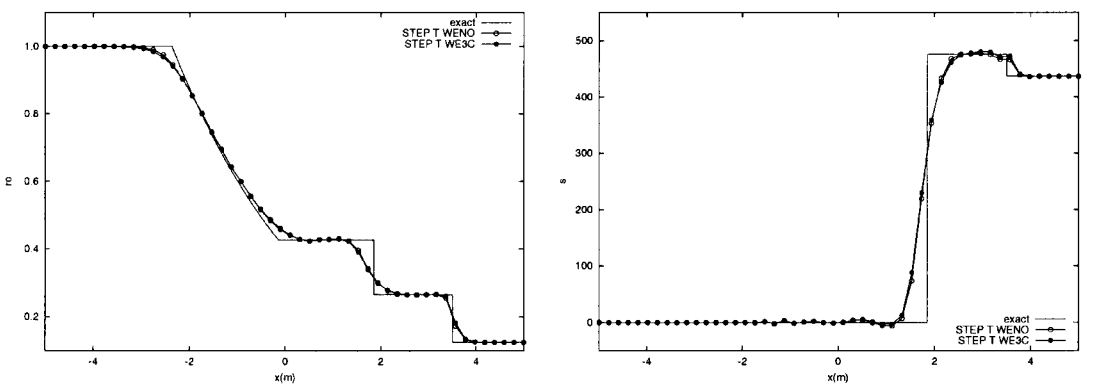

Density ρ Entropy s

Figure 11. Numerical solution of Sod's problem with the DUAL method and the implicit T time scheme for $N = 50$ and CFL $= 1.0$. Comparison of the WENO and WE3C convective schemes.

The resolution of the iterative ILU system can be visualized from the spectrum of the amplification matrix defined by $G = I - M^{-1}C$. In the case TVD or WE3C schemes are used, the ILU decomposition is exact so that the spectrum of the associated iterative amplification matrix only depends on the precision of the machine. Their spectral radius $\rho(G)$ is then of the order of 10^{-16}. For the WENO scheme, the influence of the iterative resolution and the time scheme on the spectrum is shown in Figure 12. Eigenvalues of the amplification matrix at time $t = 1$ are plotted in the complex z-plane. The results obtained with the ER, T and I3 time scheme and the STEP and the DUAL approach are presented. For both the STEP and DUAL approach, the fastest resolution of the ILU system is obtained with the I3 scheme and the slowest one with the ER time scheme.

The effect of the dual time step Δt^* on the spectrum of the amplification matrix is also shown in Figure 12. It illustrates the fact that the DUAL approach allows a more favourable

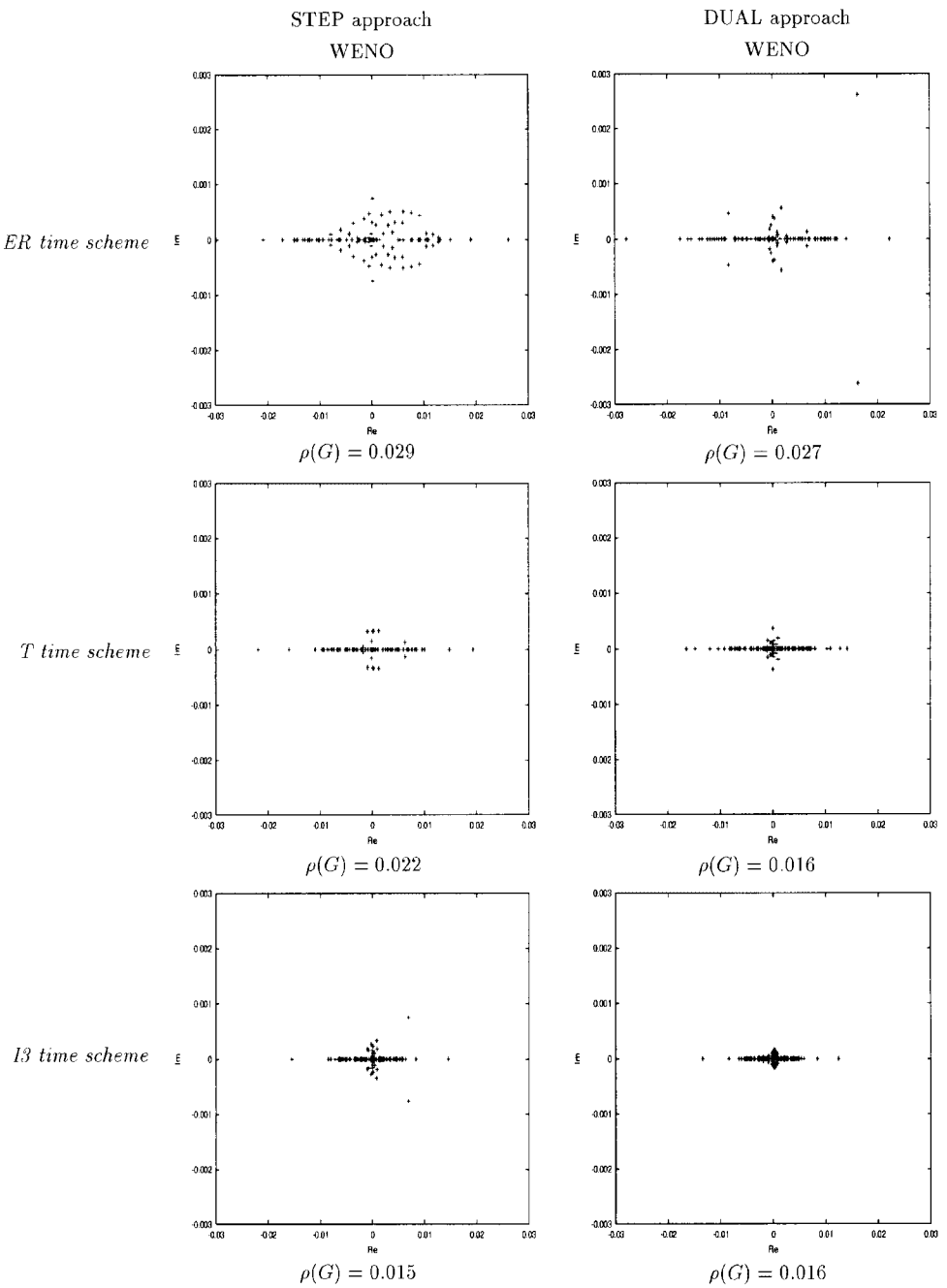

Figure 12. Eigenvalues of the amplification matrix of the ILU iterative method at time $t=1$ presented in the complex z-plane. Comparison of the ER, T and I3 time scheme using the STEP and the DUAL method ($N=50$ and CFL $=1.0$, $\Delta t^* \sim 10\Delta t^{n+1}$). The spectral radius $\rho(G)$ is also indicated under each figure.

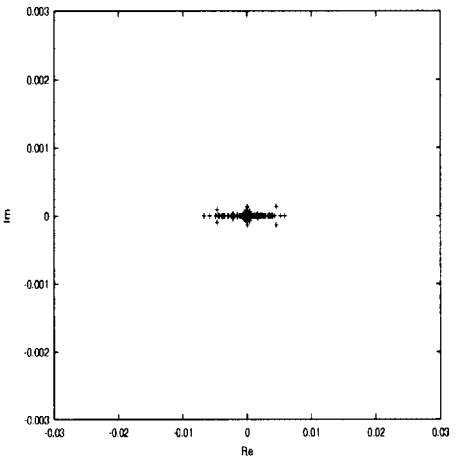

Figure 13. Influence of the Δt^* value on the amplification matrix spectrum of the ILU iterative method presented in the complex z-plane. Results obtained with the T time scheme and the DUAL approach ($N = 50$, CFL $= 1.0$, $\Delta t^* \sim \Delta t^{n+1}$).

matrix condition than the STEP approach, leading to a faster ILU resolution of the iterative system. When Δt^* is large, the behaviour of the ILU system of the DUAL approach comes close to the STEP one. When Δt^* is small, the ILU system is resolved faster and the spectral radius goes to zero (see Figure 13). For the ILU to be efficient, Δt^* has to be as small as possible.

The dual time step Δt^* in Figure 12 is the one retained in this study and is about 10 times Δt^{n+1}. The Δt^* is first calculated with the time-steady CFL criteria corresponding to the unsteady one applied for Δt^{n+1}, so that Δt^{n+1} is the minimal value of the Δt^* over all mesh points and at each iteration. The steady resolution of the dual equation, Equation (14), is performed by the unconditionally stable implicit Euler scheme, so that Δt^* can be raised and its resolution accelerated. A multiplicative factor of 10 has been found as a good compromise in this study. The ILU spectrum corresponding to the T time scheme with $\Delta t^* \sim \Delta t^{n+1}$ is shown in Figure 13 and can be compared with the corresponding one in Figure 12 where $\Delta t^* \sim 10\Delta t^{n+1}$. The residual evolution of the resolution of Equation (14) is shown in Figure 14. The convergence is clearly faster for $\Delta t^* \sim 10\Delta t^{n+1}$ than for $\Delta t^* \sim \Delta t^{n+1}$.

The influence of the time scheme on the implicit operator can be visualized by the spectrum of the amplification matrix factor defined by $G = I - \Delta t^{n+1} C$. It characterizes the amplification factor of the departure of the implicit operator from the Euler explicit scheme. Eigenvalues are plotted in the complex z-plane and the spectrum evolves in time with the unsteady solution. The spectrum at $t = 1.0$ for the STEP and DUAL approaches for WENO and TVD schemes are shown in Figure 15. The unit circle $|z| = 1$ delimits the stability area. Eigenvalues of the ER time scheme spectrum are outside the stability circle for every approach. Their frequencies are not smoothed by the implicit operator, leading to an unstable behaviour as observed during our computations. For the T and I3 schemes, where the iterative method is well conditioned, the most unstable modes correspond to the closest eigenvalues to the unit circle. A compact spectrum is important for the resolution of unsteady equations to prevent the implicit time

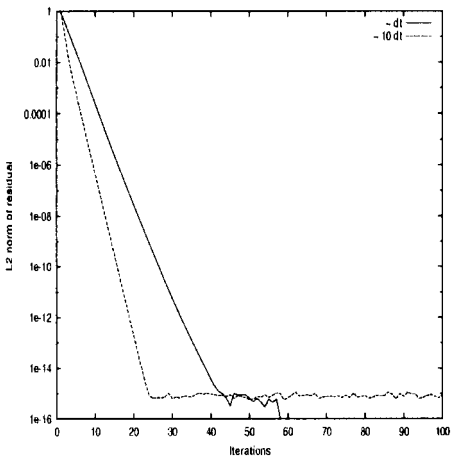

Figure 14. Influence of the dual time step Δt^* on the convergence of Equation (14). The residuals obtained with the T time scheme and the DUAL approach are shown ($N = 50$, $\mathrm{CFL} = 1.0$, $\Delta t^* \sim \Delta t^{n+1}$ and $\Delta t^* \sim 10\Delta t^{n+1}$).

scheme to behave like a low-frequency filter, especially in a large eddy simulation context. The shape of the spectrum for TVD and WENO schemes evolve in a very similar way from one time scheme to another. For a given time scheme, differences are observed between the spectrum associated to the TVD convective scheme and the WENO one. More eigenvalues are detached from the core of the spectrum in the WENO case than in the TVD case. Differences between the STEP and the DUAL approaches are found negligible, showing that the implicit operator behaves in a similar way for the same convective scheme.

An evaluation of the relative costs of the implicit and explicit resolutions can be obtained by estimating the averaged CPU time needed for one physical time step. Figures 16 and 17 show the CPU time evolution with increasing CFL number of the TVD and WENO scheme for every time integration method. As expected, the cost of the STEP and explicit schemes do not depend on CFL number. The cost of the implicit integration is more than 10 times higher than the cost of the explicit one. The STEP approach increases the average CPU time by only a factor 2 compared with the explicit solver, but it is shown that the non-linearities are not well resolved by this approach. This suggests that the STEP approach is not well suited for unsteady problems. A comparison of the NWT and the DUAL method shows that for a dual time step about $\Delta t^* \sim 10\Delta t^{n+1}$ the CPU time is faster or equivalent of the NWT approach. The cost of the dual approach can be decreased by choosing a smaller dual time step Δt^*. According to these results, it would be necessary to work with CFL numbers greater than 20 in order to balance the implicit resolution cost.

Lax's explicit solver: The general behaviour of the explicit TVD and WENO schemes in the Lax problem are very similar. The Lax problem is characterized by a higher shock intensity than in Sod's problem. However, no specific correction is applied to the contact discontinuity. Its slope could be improved by introducing a function correction or working with a $k > 4$ WENO scheme [13]. Results obtained with the Runge–Kutta explicit time scheme are shown in Figure 18 for $\mathrm{CFL} = 0.5$ and 1.0. It is observed that a higher CFL number decreases the accuracy of the expansion wave resolution.

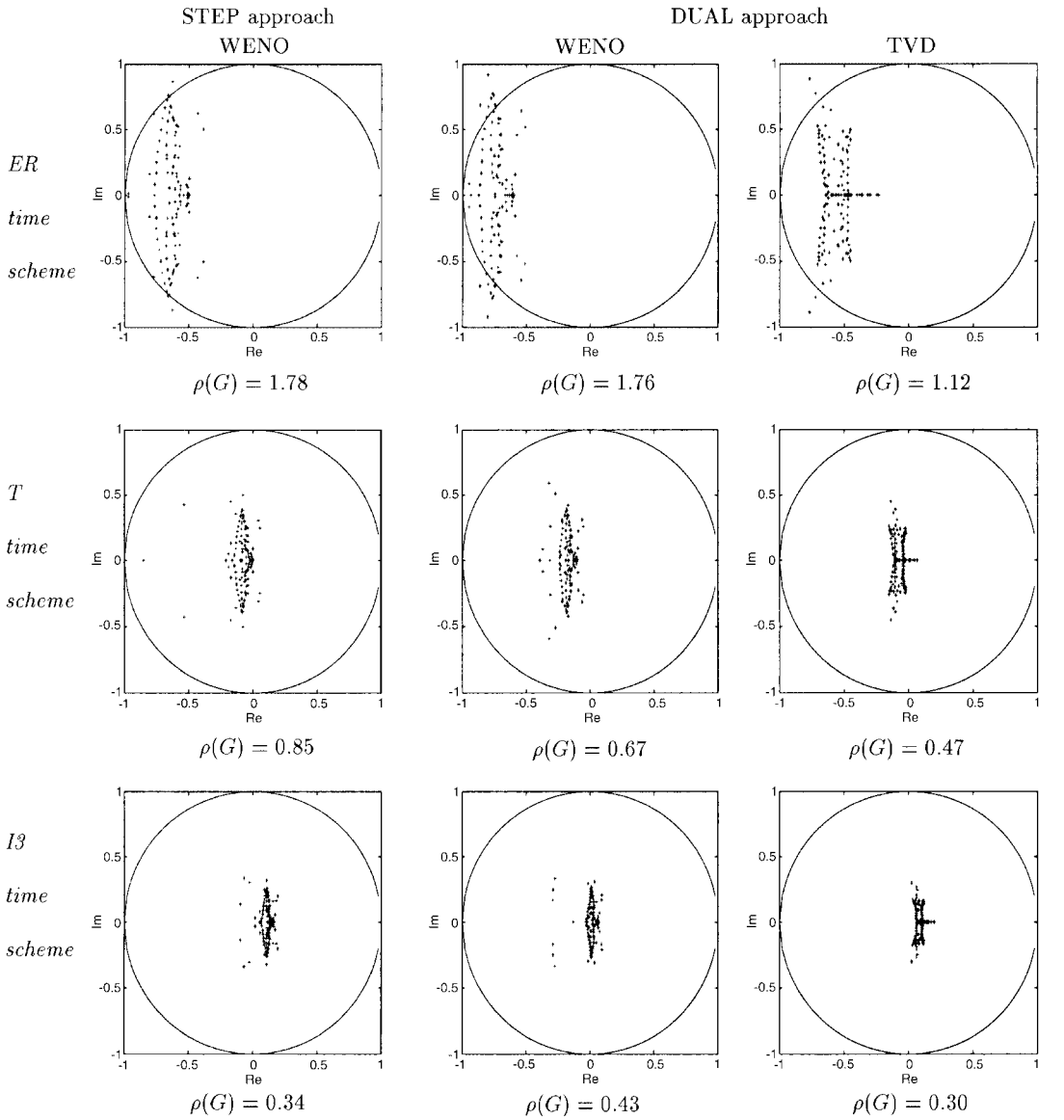

Figure 15. Spectrum of the amplification matrix in the complex z-plane at time $t = 1$. Also shown are the unit circle $|z| = 1$ and the spectral radius $\rho(G)$ ($N = 50$ and CFL $= 1.0$, $\Delta t^* \sim 10\Delta t^{n+1}$).

Lax's implicit solver: The implicit resolution of Lax's problem leads to the same hierarchy of the different methods as with the Sod case. The DUAL approach in combination with the T time scheme gives the best results as shown in Figures 19 and 20. Similar results can be obtained with the implicit DUAL method at CFL $= 1.5$ and the explicit Runge–Kutta solver at CFL $= 0.5$ when using the WENO scheme. The implicit WENO solver proposed here correctly

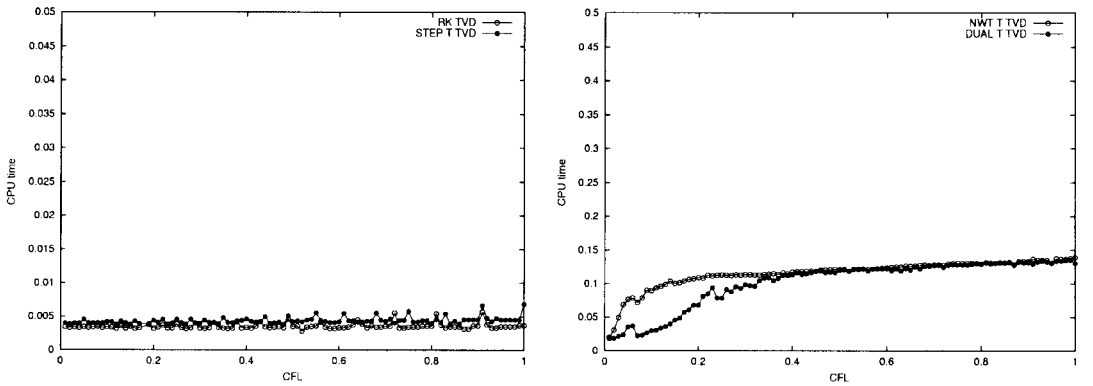

Figure 16. Evolution of the average CPU time with the CFL number for the TVD scheme for $N = 50$.

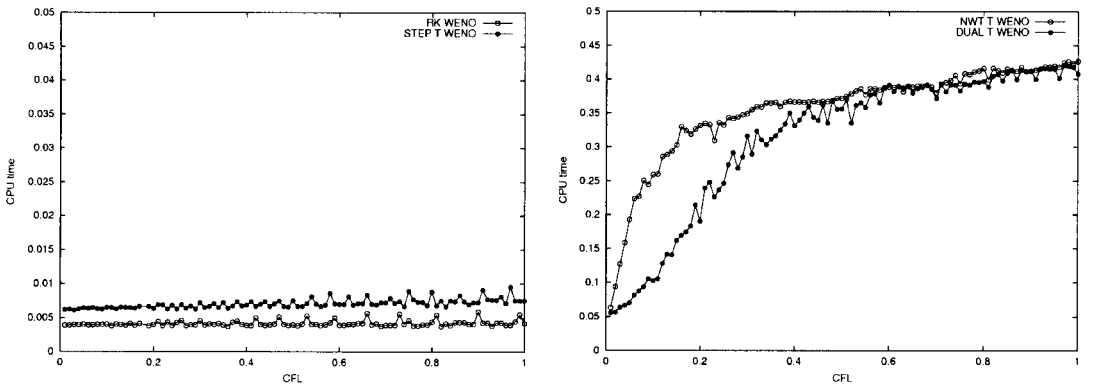

Figure 17. Evolution of the average CPU time with the CFL number for the WENO scheme for $N = 50$.

captures the shock discontinuity and conserves the shock velocity in the development of the unsteady solution.

4.2. 1D shock-entropy wave interaction

In the next example, a $M = 3$ shock wave moving from left to right interacts with a sine entropy wave represented by density fluctuations [13]. This case is suitable for testing high-order schemes as the solution involves shocks as well as complicated smooth flow features. The computational domain is the interval $[-5, 5]$ and the initial condition is

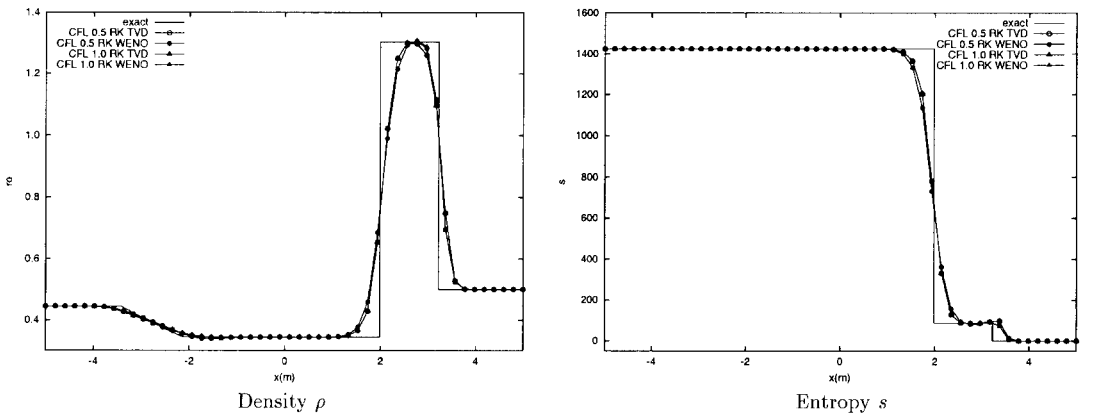

Figure 18. Numerical solution of Lax's problem with the explicit Runge–Kutta time scheme and the TVD and WENO spatial schemes for $N = 50$ and CFL $= 0.5$ and 1.0.

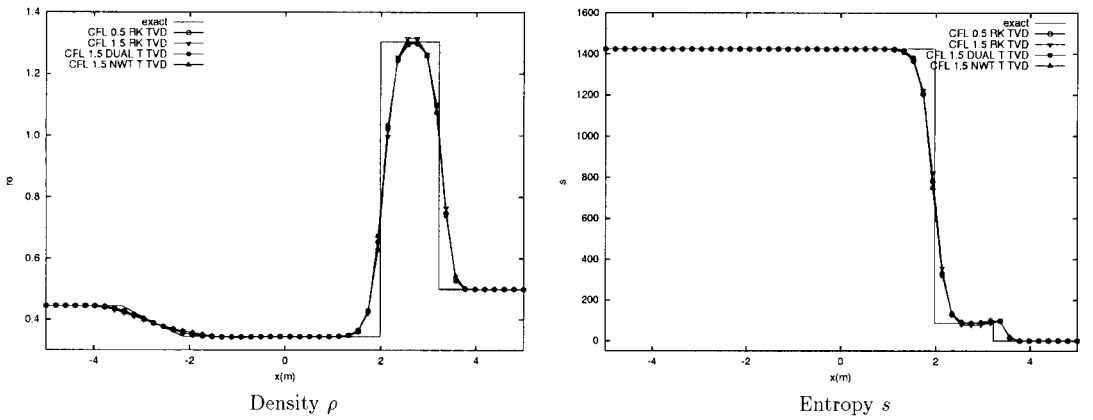

Figure 19. Numerical solution of Lax's problem with the TVD spatial scheme with $N = 50$. Comparison of the explicit RK (CFL $= 0.5$ and 1.5) and the implicit NWT and DUAL (CFL $= 1.5$) time scheme.

the following:

$$\rho = 3.85714 \;\; u = 2.629369 \;\; p = 10.33333 \text{ when } x < -4$$

$$\rho = 1 + \varepsilon \sin(kx) \;\; u = 0 \;\; p = 1 \text{ when } x \geqslant -4$$

where ε and k are, respectively, the amplitude and the wave number of the entropy wave. When the amplitude of the entropy wave is weak compared to the shock strength, for example $\varepsilon = 0.2$ and $k = 5$, a sound wave is generated behind the shock. The entropy fluctuations are amplified as they pass through the shock. The numerical solutions shown here are calculated up to a time of $t = 1.8$. A reference solution is obtained on 18,000 grid points using the WENO scheme and the time explicit resolution and is considered to be very close to the exact solution in the next comparisons.

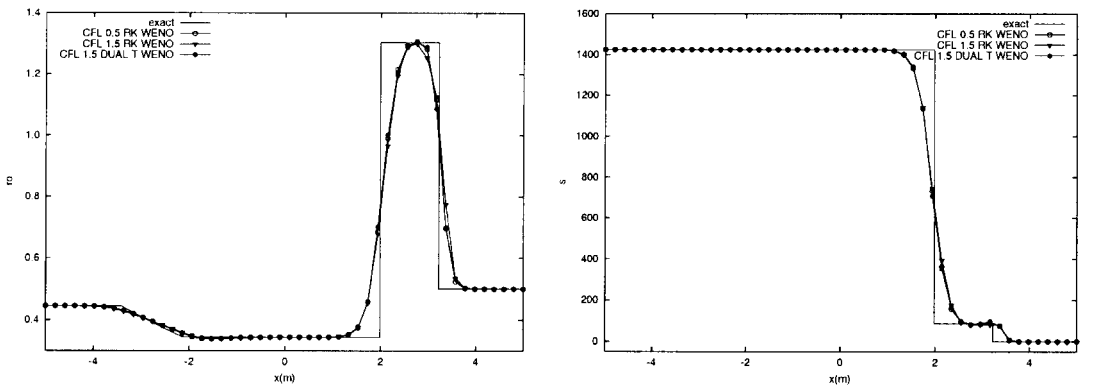

Density ρ Entropy s

Figure 20. Numerical solution of Lax's problem with the WENO convective scheme with $N = 50$. Comparison of the explicit RK (CFL = 0.5 and 1.5) and the implicit DUAL (CFL = 1.5) time scheme.

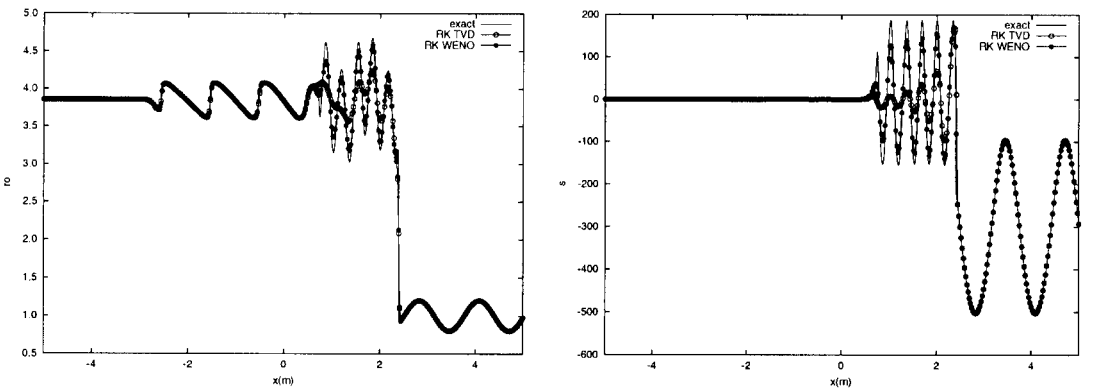

Density ρ Entropy s

Figure 21. Numerical solution of the shock-entropy wave interaction with the explicit RK time scheme with $N = 400$ and CFL = 1.0. Comparison of the exact solution with the TVD and WENO spatial schemes.

Explicit solver: Results obtained with the explicit time scheme are shown in Figure 21. The numerical solution obtained with CFL = 1.0 is identical to the one obtained with CFL = 0.5. High frequency oscillations are better captured by the WENO scheme than by the TVD scheme. The TVD scheme is too dissipative in areas where shocks are weak, which can be attributed to the use of limiters in the TVD approach. The advantage of the WENO over the TVD schemes for this kind of problems is then obvious.

Implicit solver: In Figures 22 and 23 the implicit resolution is compared with the DUAL time-stepping method for the TVD and WENO schemes, respectively. The explicit and implicit solutions obtained with the WENO scheme are very similar. The implicit method developed here allows to capture correctly the shock discontinuity and does not affect its velocity.

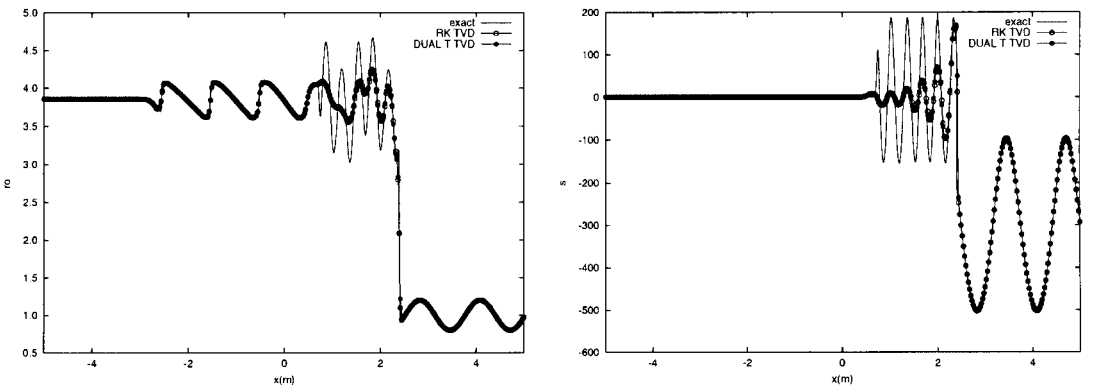

Density ρ Entropy s

Figure 22. Numerical solution of the shock-entropy wave interaction with the TVD spatial scheme with $N = 400$ and $\mathrm{CFL} = 1.0$. Comparison of the explicit RK and the implicit T time scheme with the DUAL method.

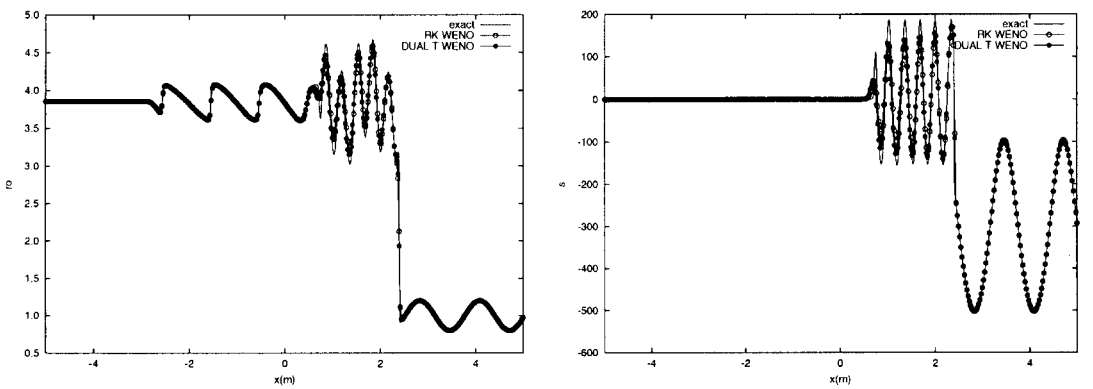

Density ρ Entropy s

Figure 23. Numerical solution of the shock-entropy wave interaction with the WENO spatial scheme with $N = 400$ and $\mathrm{CFL} = 1.0$. Comparison of the explicit RK and the implicit T time scheme with the DUAL method.

5. CONCLUSIONS

The resolution of unsteady hyperbolic equations to solve problems involving shocks and complicated smooth structures has been studied with TVD and WENO schemes. In the cases treated here, the fifth-order WENO scheme allows to capture the discontinuity in the solution more accurately than the TVD scheme. Explicit results obtained with the TVD and WENO schemes are served here as references for comparison with the implicit solver. No entropy correction has been introduced in the TVD scheme. Oscillations were observed in the WENO solution on the entropy evolution before the expansion wave. This can be due to the fact that the spatial discretization order is higher than the time discretization, leading to a more

restrictive CFL condition than given by a linear stability analysis preserving non-oscillating properties.

Implicit resolution of the Euler equation is performed through a linearization of the convective fluxes in order to build the implicit operator. The explicit form of the second-order TVD scheme involving flux limiters expands on 5 points in each direction whereas its stencil expands on only 3 points when no limiters are taken into account. This scheme is therefore classically linearized in a compact form in order to build an implicit operator formed by a block three diagonal matrix. The resolution of the system is then performed by an ILU method. In the case of the fifth-order WENO scheme, the construction of the implicit operator proposed in this study is straightforward. The scheme does not involve any limiters so that the implicit operator can be written in a way similar to its explicit form. The implicit operator is, therefore, involving the Jacobian matrix of the convective fluxes. The interpolation on the implicit candidate stencils is made on criteria based on previous time-step solution, so that it is not interesting to implicit only the first three diagonal blocks in the operator and explicit the remaining part. This feature is an advantage of the proposed formulation when unsteady solutions involving sharp discontinuities are computed. The smooth WENO criteria is indeed always based on a time consistent solution. Moreover, the semi-implicit form could lead to an erroneous shock velocity prediction for high shock intensities. The resolution of non-linearities is, therefore, important in order to verify the weight criteria at each physical time step. This leads to a resolution of the implicit operator based on dual time stepping method. The results obtained with this method proved to be better than with the one-step approach showing that it is necessary to properly solve the non-linearities for unsteady solutions. The implicit scheme also keeps the WENO ability of capturing both shocks and high-order frequency flow structures. This property is particulary interessant in the perspective of Large Eddy Simulations of unsteady compressible flows in order to get a better resolution of the flow field.

Generally, the implicit solver allows a higher CFL number than the explicit solver. Typically, explicit results obtained for a CFL number of 0.5 are identical to the implicit solution calculated at a CFL number of 1.0. The implicit solver is, however, more expensive in terms of CPU time per physical time step. The additional costs of the implicit resolution developed here would require a CFL number of about 20 to obtain the CPU time of the explicit solver.

The method presented here for one-dimensional problems on curvilinear meshes can be easily extended to multiple space dimensions. The implicit operator associated to a WENO scheme for a three-dimensional problem results in a 5×5 block matrix of 19 diagonals so that the ILU solver can easily be extended to this configuration. The relaxation solver used in this study could be improved to get a faster implicit solver. For example, the ILU method used here may be used as a pre-conditioner of a more efficient relaxation method, like a conjugate gradient method. This approach is known to be more efficient and would be therefore a better choice than the ILU method in multi-dimensional problems.

REFERENCES

1. Karlsen KH, Lie KA, Natvig JR, Nordhaug NF, Dahle HK. Operator splitting methods for systems of convection-diffusion equations: Nonlinear error mechanisms and correction strategies. *Journal of Computational Physics* 2001; **173**:636–663.
2. Harten A. High resolution schemes for hyperbolic conservation laws. *Journal of Computational Physics* 1983; **49**:357–393.
3. Colella P, Woodward PR. The piecewise parabolic method (PPM) for gas dynamical simulations. *Journal of Computational Physics* 1984; **54**:115–173.

4. Yee HC. On the implementation of a class of upwind schemes for system of hyperbolic conservation laws. *Technical Report* 86839, NASA TM, 1985.
5. Chakravarthy SR, Osher S. Very high order accurate TVD schemes. *AIAA Paper*, 85-0363, 1985.
6. Hirsch C. *Numerical Computation of Internal and External Flows*. Wiley: New York, 1989.
7. Van Leer B. *Journal of Computational Physics* 1974; **14**:361–370.
8. Sweby PK. High order resolution schemes using flux limiters for hyperbolic conservation laws. *SIAM Journal of Numerical Analysis* 1984; **21**:995–1011.
9. Roe PL. Some contributions to the modelling of discontinuous flows. *Lecture Notes in Applied Mathematics* 1985; **22**:163–193.
10. Yee HC. Construction of explicit and implicit symmetric TVD schemes and their applications. *Journal of Computational Physics* 1987; **68**:151–179.
11. Harten A, Osher S, Engquist B, Chakravarthy S. Uniformly high order essentially non-oscillatory schemes III. *Journal of Computational Physics* 1987; **71**:231–303.
12. Shu WC, Osher S. Efficient implementation of essentially non-oscillatory shock capturing schemes. *Journal of Computational Physics* 1988; **77**:439–471.
13. Shu WC, Osher S. Efficient implementation of essentially non-oscillatory shock capturing schemes II. *Journal of Computational Physics* 1989; **83**:32–78.
14. Liu XD, Osher S, Chan T. Weighted essentially nonoscillatory schemes. *Journal of Computational Physics* 1994; **115**:200–212.
15. Jiang G, Shu CW. Efficient implementation of weighted ENO schemes. *Journal of Computational Physics* 1996; **126**:202–228.
16. Chen Y, Yang S, Yang J. Implicit weighted essentially non-oscillatory schemes for the incompressible Navier–Stokes equations. *International Journal for Numerical Methods in Fluids* 1999; **31**:747–765.
17. Yang J, Perng Y, Yen R. Implicit weighted essentially non-oscillatory schemes for the compressible Navier–Stokes equations. *AIAA Journal* 1999; **39**(11):2082–2090.
18. Gottlieb S, Shu CW. Total variation diminishing Runge–Kutta schemes. *Technical Report* 50, ICASE, 1996.
19. Caruelle B. Simulations d'écoulements instationnaires turbulents en aérodynamique: application à la prédiction du phénoméne de tremblement. *Ph.D. Thesis*, Toulouse, 2000.
20. Weber C. Développement de méthodes implicites pour les équations de Navier–Stokes moyennées et la simulation des grandes échelles: Application á l'aérodynamique externe. *Ph.D. Thesis*, Toulouse, 1998.
21. Beam R, Warming R. Altering direction implicit methods for parabolic equations with a mixed derivative. *SIAM Journal on Scientific and Statistical Computing* 1980; **1**:131–159.
22. Roe PL. Approximate Riemann solvers, parameter vectors, and difference schemes. *Journal of Computational Physics* 1981; **43**:357–372.
23. Harten A, Engquist B, Osher S, Chakravarthy S. Uniformly high order accurate essentially non oscillatory schemes. *Journal of Computational Physics* 1987; **71**:231–303.
24. Yee HC. Explicit and implicit compact high-resolution shock-capturing methods for multidimensional Euler equations i: Formulation. *Technical Report* 110364, NASA TM, 1995.
25. Yee HC, Harten A. Implicit TVD schemes for hyperbolic conservation laws in curvilinear co-ordinates. *AIAA Journal* 1985; **25**(2):266–274.
26. Cadiou A, Tenaud C. Schémas TVD et WENO explicites et implicites pour la résolution des équations d'euler: Apllication au tube á choc. *Technical Report* 2001-08, Notes et Doc LIMSI, 2001.
27. Shu CW. Essentially non-oscillatory and weighted essentially non-oscillatory schemes for hyperbolic conservation laws. *Technical Report* 65, ICASE, 1997.
28. Sod G. A survey of finite difference methods for systems of non-linear hyperbolic conservation laws. *Journal of Computational Physics* 1978; **27**(1):1–31.
29. Lax PD. Weak solutions of nonlinear hyperbolic equations and their numerical computation. *Communications on Pure and Applied Mathematics* 1954; **7**:159–193.

